This article has been accepted for publication in a future issue of this journal, but has not been fully edited. Content may change prior to final publication. Citation information: DOI 10.1109/TEC.2018.2881710, IEEE Transactions on Energy Conversion

Reduced-order Aggregate Model for Parallel-connected Single-phase Inverters

Victor Purba, *Student Member*, *IEEE*, Brian B. Johnson, *Member*, *IEEE*, Miguel Rodriguez, Saber Jafarpour, *Member*, *IEEE*, Francesco Bullo, *Fellow*, *IEEE*, and Sairaj V. Dhople, *Member*, *IEEE*

***Abstract*—This paper outlines a reduced-order aggregate dynamical model for parallel-connected single-phase grid-connected inverters. For each inverter, we place no restrictions on the converter topology and merely assume that the ac-side switch-averaged voltage can be controlled via pulse width modulation. The ac output of each inverter interfaces through an LCL filter to the grid. The closed-loop system contains a phase locked loop for grid synchronization, and real- and reactive-power control are realized with inner and outer PI current- and power-control loops. We derive a necessary and sufficient set of parametric relationships to ensure that a reduced-order aggregated state-space model for an arbitrary number of such paralleled inverters has the same model order and structure as any single inverter. We also present reduced-order models for the settings where the real- and reactive-power setpoints are different and where the inverters have different power ratings. We anticipate the proposed model being useful in analyzing the dynamics of large collections of parallel-connected inverters with minimal computational complexity. The aggregate model is validated against measurements obtained from a multi-inverter experimental setup consisting of three $750\,\mathrm{VA}$ paralleled grid-connected inverters, hence establishing robustness of the analytical result to parametric variations seen in practice.**

***Index Terms*—Model reduction, phase-locked loop, single-phase inverter, voltage-source inverter.**

I. Introduction

Rapid adoption of renewable sources of generation (e.g., photovoltaic (PV) energy conversion systems) and flexible loads (e.g., electric vehicles) has increased the number of power electronics inverters installed on the ac power grid. Scalable models that present limited computational burden will be critical to model and analyze the collective dynamics of large numbers of inverters in next-generation power networks [1]. To motivate the need for modeling strategies that can be applied to complex inverter systems, consider the relatively small island of Oahu which already has over $800,000$ microinverters [2]. This number is expected to grow significantly as Hawaii aims to meet the goal of obtaining 100% of its energy from renewable sources [3]. Although the Hawaiian system is at the forefront of renewable adoption, it presents a glimpse at anticipated worldwide trends [4].

The disparity in ratings between individual inverters (no larger than a few MVA) and synchronous generators (several hundred MVA) implies that if the same net load were served with power electronics instead of generators, there would be an orders-of-magnitude increase in the number of energy-conversion interfaces (from a few thousand generators to potentially millions of inverters across a large-scale synchronous grid). Evaluating the stability and resilience of future power networks will therefore require accurate dynamical models for large collections of inverters that present limited computational burden. However, development of such models is challenged by the complexity of inverter dynamics (for instance, the particular model we examine in this paper is nonlinear, and composed of 16 states) and the sheer number of inverters that will eventually be commonplace on the ac power grid. To address the challenge of model complexity in multi-inverter systems, we propose an aggregate reduced-order state-space model for an arbitrary number of single-phase grid-tied inverters connected in parallel. While our analytical result is presented for identical inverters, we experimentally validate our findings which immediately establishes robustness to parametric variations that are likely to be seen in practice. We also present extensions of the main result on model reduction to cover cases when the power setpoints of the inverters are all different and the power ratings of the inverters are all different.

We examine the ac-timescale dynamics of a single-phase voltage source inverter (VSI) with an output LCL filter. To ensure broad applicability across VSI topologies, we only assume that the switch-averaged voltage across the ac terminals is controllable via pulse width modulation and we neglect switch-level dynamics. The control architecture is composed of an inner current-control loop, an outer power-control loop, and a phase locked loop (PLL) for grid synchronization. This filter and control architecture are prototypical and it ensures broad applicability of the results. The state-space model that captures the dynamics of the inverter is composed of 16 states. The contributions of the paper are threefold:

1) For a parallel collection of N inverters, we derive a *necessary and sufficient* set of parametric relationships for an aggregate reduced-order inverter model to have a state-space model with the same structure and model order (i.e., composed of the same 16 states referenced above) as any single inverter in the collection. (Figure 1

V. Purba and S. V. Dhople are with the Department of Electrical and Computer Engineering at the University of Minnesota, Minneapolis, MN (email: {purba002,sdhople}@umn.edu); B. B. Johnson is with the Department of Electrical and Computer Engineering at the University of Washington, Seattle, WA (e-mail: brianbj@uw.edu); M. Rodriguez was with the Power Systems Engineering Center at the National Renewable Energy Laboratory, Golden, CO (now with Advanced Micro Devices, Inc., Fort Collins, CO, e-mail: miguel.rodriguez@amd.com); S. Jafarpour and F. Bullo are with the Department of Mechanical Engineering at the University of California, Santa Barbara, Santa Barbara, CA (email: {saber.jafarpour, bullo}@engineering.ucsb.edu). This work was supported in part by the U.S. Department of Energy under Contract No. DE-EE0000-1583 and the National Science Foundation under grant 1453921.

This article has been accepted for publication in a future issue of this journal, but has not been fully edited. Content may change prior to final publication. Citation information: DOI 10.1109/TEC.2018.2881710, IEEE Transactions on Energy Conversion

illustrates the idea.)

2) We derive parameters for an aggregate reduced-order model (with the same order and stucture as any individual inverter) for the case where the real and reactive-power setpoints for the inverters are all different.
3) We derive parameters for an aggregate reduced-order model (with the same order and structure as any individual inverter) for the case where the power ratings of the inverters are all different.

In general, the identical state-space model structure implies that from a topological vantage point, the aggregated equivalent model also maps to an inverter with an LCL filter, an inner current-control loop, an outer power-control loop, and a PLL for grid synchronization, *except* with different filter parameters and control gains. With reference to contribution 1) above, while some aspects of the aggregate model appear intuitive in hindsight (e.g., given the parallel arrangement, the output inductances in the aggregate model are $1/N$ times those in any individual inverter), the parametric dependencies in pertinent control gains are not. What is more, the fact that the parametric relationships we derive in 1) are necessary *and* sufficient implies that we exhaustively enumerate *all* alternative possibilities to obtain a structurally similar reduced-order model. Contributions in 2) and 3) follow as corollaries to the main result in 1) and enable extending the result to obtain aggregate models under heterogeneous settings that are likely to be noticed in practice. Finally, we believe that the general state-space modeling formulation and the proof strategy can be extended to other control strategies to establish similar aggregate models.

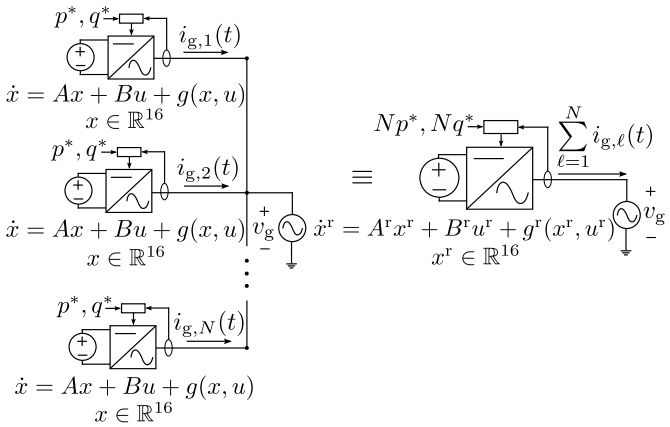

Figure 1: (left) System of N parallel grid-connected single-phase inverters. Controller for the ℓ-th inverter regulates the injected grid current, $i_{\mathrm{g},\ell}(t)$ to deliver (the commanded) real power p^* and reactive power q^* into the grid terminals. We examine a prototypical 16-th order inverter dynamical model, which implies that the parallel system is described by a $16N$-order dynamical model. (right) Aggregated equivalent has state-space model with the same dimension and structure as any individual inverter, i.e., it is described by a 16-th order dynamical model, and A^{r}, B^{r} and $g^{\mathrm{r}}(\cdot,\cdot)$ have the same form as A, B and $g(\cdot,\cdot)$. We derive the model parameters for the aggregated-inverter filter and controllers such that with power inputs Np^* and Nq^*, the instantaneous injected grid current is the sum of all individual currents $\sum_{\ell=1}^{N} i_{\mathrm{g},\ell}(t)$ (other states scale systematically as well).

A majority of prior literature pertaining to model reduction for energy conversion interfaces has understandably focused on the dynamics of fossil-fuel-driven synchronous generators [5]–[9]. More recently, there has been increased attention devoted to aggregate models for wind-turbines in utility-scale collector systems [10], electric vehicles [11], and demand response systems [12]. However, these are focused at a macro level that disregards the dynamics at faster time scales which arise from inverter filters and time-domain controllers. With regard to inverter dynamics, most of the related literature has predominantly focused on reduced-order models for *individual* grid-connected [13], islanded [14]–[16], and resonant inverters [17]. (Tangentially related is literature on model reduction of dc-dc converters [18]–[20] and induction machines [21], [22].) Model-reduction methods focused on *collections* of inverters have been limited to islanded settings [23], [24] and inverters with virtual-inertia emulation [25]. Both are application domains where inverters are controlled to emulate the dynamics of synchronous generators, and therefore, there is a natural translation of classical model-reduction methods for synchronous generators mentioned previously.

Given the landscape of related work discussed above, this work addresses a key gap in the literature pertaining to the dynamics of grid-connected multi-inverter systems. This paper significantly builds upon and extends our preliminary work in [26] where we developed similar aggregated models for parallel-connected *three-phase* inverters. Here, we examine the (admittedly different) filter and controller dynamics for *single-phase* inverters which will conceivably be more dominant in number in future distribution networks. As a further and important contribution, we provide experimental validation of our approach with a multi-inverter setup composed of three 750 VA grid-tied single-phase inverters. We note that the parallel aggregation approach proposed here provides the base for a broader set of aggregation techniques that can account for the network connection of the inverters. For instance, in [27] three-phase inverters are transferred to an auxiliary bus with the aid of auxiliary transformers, and subsequently aggregated using the parallel aggregation approach discussed here.

The remainder of this manuscript is organized as follows: In Section II, we establish mathematical notation and describe the grid-tied single-phase inverter model. The reduced-order model for a collection of these inverters connected in parallel is derived in Section III. We validate the model-reduction method by comparing numerical simulation results with results from the experimental prototype in Section IV. Finally, concluding remarks and directions for future work are in Section V.

II. Preliminaries and Inverter Dynamical Model

In this section, we first introduce mathematical notation used in the manuscript. Then we describe the single-phase inverter model, and develop a standard state-space model representation.

A. Notation

For a vector $x \in \mathbb{R}^N$, $\mathrm{diag}(x) \in \mathbb{R}^{N\times N}$ returns a diagonal matrix with diagonal entries composed of entries of x. All-ones and all-zeros vectors of length N are denoted by 1_N and

This article has been accepted for publication in a future issue of this journal, but has not been fully edited. Content may change prior to final publication. Citation information: DOI 10.1109/TEC.2018.2881710, IEEE Transactions on Energy Conversion

0_N, respectively. Finally, $0_{M\times N}$ denotes the all-zeros matrix of size M-by-N.

B. Dynamical Model of Single-phase Inverter

A block diagram of the grid-connected single-phase inverter is illustrated in Fig. 2. The PLL is designed to track the instantaneous angle of the grid voltage at the point of common coupling, the power controller regulates the real and reactive power delivered into the ac grid, and the current controller governs the current delivered by the switch terminals. This model represents a prototypical implementation in a single-phase grid-connected setting and captures all relevant ac-side system dynamics. Since the focus of the paper is at the ac-side point of common coupling, dynamics of the dc-link and any other converter stages that precede the dc-link are neglected. We briefly overview the reference-frame transformations and the dynamics of the filter and controllers next.

Reference-frame Transformations: The controllers illustrated in Fig. 2 are implemented in the dq domain. To enable this, the Hilbert transform [28] (denoted by $G_{\pi/2}$) is first utilized to generate orthogonal signals with quarter-cycle phase lag for each sinusoidal measurement, i.e., it yields signals in the $\alpha\beta$ domain [29]. Each signal and its corresponding phase-shifted counterpart is subsequently processed by an $\alpha\beta$ to dq transformation. The dq signals are then used in the PLL and current controller. Note that although the above formulation utilizes the Hilbert transform as a means of generating quarter-cycle phase-shifted waveforms, these signals can also be realized with a quarter-cycle delay buffer or an all-pass filter with appropriate phase response. The remainder of the manuscript focuses exclusively on the Hilbert transform without loss of generality.

The transfer function of the Hilbert transform is given by

$$G_{\pi/2}(s) = \frac{\omega_{\mathrm{PLL}} - s}{\omega_{\mathrm{PLL}} + s}, \tag{1}$$

where ω_{PLL} is the frequency returned by the PLL. As shown in Fig. 2, we will consider the measured signal to be the α-component, and the corresponding output of the Hilbert transform as the β component. Next, signals in the $\alpha\beta$ reference frame (x^α, x^β) are transformed to the dq reference-frame $(x^{\mathrm{d}}, x^{\mathrm{q}})$ with the following rotation matrix [29]:

$$\begin{bmatrix} x^{\mathrm{d}} \\ x^{\mathrm{q}} \end{bmatrix} = \begin{bmatrix} \cos\delta & \sin\delta \\ -\sin\delta & \cos\delta \end{bmatrix} \begin{bmatrix} x^\alpha \\ x^\beta \end{bmatrix}, \tag{2}$$

where δ is the instantaneous angle generated by the PLL. As seen in Fig. 2, the PLL is in feedback with the dq transformation. The role of the PLL is to modulate the value of the PLL angle, δ, such that the d-axis component of the grid voltage, $v_{\mathrm{g}}^{\mathrm{d}}$, is driven asymptotically to zero. From the definition of the α- and β-components of v_{g} and the dq transformation in (2), it can be shown that if $v_{\mathrm{g}}^{\mathrm{d}} = 0$, then δ is the instantaneous phase angle of v_{g}. (See Appendix A for a short derivation.)

Controller and Filter Dynamics: The internal controllers in the PLL comprise a low-pass filter with cut off frequency $\omega_{\mathrm{c,PLL}}$ and a PI controller with proportional and integral gains given by k_{PLL}^p and k_{PLL}^i, respectively. The PLL dynamics are given by

$$\frac{d}{dt}v_{\mathrm{PLL}} = \omega_{\mathrm{c,PLL}}(v_{\mathrm{g}}^{\mathrm{d}} - v_{\mathrm{PLL}}), \tag{3a}$$

$$\frac{d}{dt}\phi_{\mathrm{PLL}} = -v_{\mathrm{PLL}}, \tag{3b}$$

$$\frac{d}{dt}\delta = \omega_{\mathrm{nom}} - k_{\mathrm{PLL}}^p v_{\mathrm{PLL}} + k_{\mathrm{PLL}}^i \phi_{\mathrm{PLL}} =: \omega_{\mathrm{PLL}}, \tag{3c}$$

$$\frac{d}{dt}v_{\mathrm{g}}^\beta = \omega_{\mathrm{PLL}}(v_{\mathrm{g}} - v_{\mathrm{g}}^\beta) - \frac{d}{dt}v_{\mathrm{g}}, \tag{3d}$$

where ω_{nom} is the nominal grid frequency (e.g., $2\pi \times 60$ or $2\pi \times 50$ rad/s). We apply (1) to v_{g} to obtain the dynamics of v_{g}^β in (3d), and we apply (2) to v_{g} and v_{g}^β to obtain $v_{\mathrm{g}}^{\mathrm{d}}$ which feeds into (3a). From above, we can see that $v_{\mathrm{g}}^{\mathrm{d}} = v_{\mathrm{PLL}} = 0$ in steady-state. Furthermore, when the grid frequency is ω_{nom}, it follows that $\dot{\delta} = \omega_{\mathrm{PLL}} = \omega_{\mathrm{nom}}$. Note that we assume the first derivative of v_{g}, i.e., $\frac{d}{dt}v_{\mathrm{g}}$, to be well defined.

The LCL filter is composed of inverter-side inductance L_{i}, grid-side inductance, L_{g}, and filter capacitance, C_{f}. The dynamics introduced by the LCL filter in the $\alpha\beta$ frame are given by

$$\frac{d}{dt}i_{\mathrm{i}}^\alpha = \frac{1}{L_{\mathrm{i}}}(-R_{\mathrm{i}}i_{\mathrm{i}}^\alpha + v_{\mathrm{i}}^\alpha - v_{\mathrm{f}}^\alpha), \tag{4a}$$

$$\frac{d}{dt}i_{\mathrm{i}}^\beta = \omega_{\mathrm{PLL}}(i_{\mathrm{i}}^\alpha - i_{\mathrm{i}}^\beta) - \frac{d}{dt}i_{\mathrm{i}}^\alpha, \tag{4b}$$

$$\frac{d}{dt}i_{\mathrm{g}}^\alpha = \frac{1}{L_{\mathrm{g}}}(-R_{\mathrm{g}}i_{\mathrm{g}}^\alpha + v_{\mathrm{f}}^\alpha - v_{\mathrm{g}}), \tag{4c}$$

$$\frac{d}{dt}i_{\mathrm{g}}^\beta = \omega_{\mathrm{PLL}}(i_{\mathrm{g}}^\alpha - i_{\mathrm{g}}^\beta) - \frac{d}{dt}i_{\mathrm{g}}^\alpha, \tag{4d}$$

$$\frac{d}{dt}v_{\mathrm{f}}^\alpha = R_{\mathrm{f}}\left(\frac{d}{dt}i_{\mathrm{i}}^\alpha - \frac{d}{dt}i_{\mathrm{g}}^\alpha\right) + \frac{1}{C_{\mathrm{f}}}(i_{\mathrm{i}}^\alpha - i_{\mathrm{g}}^\alpha), \tag{4e}$$

$$\frac{d}{dt}v_{\mathrm{f}}^\beta = \omega_{\mathrm{PLL}}(v_{\mathrm{f}}^\alpha - v_{\mathrm{f}}^\beta) - \frac{d}{dt}v_{\mathrm{f}}^\alpha, \tag{4f}$$

where the α-component dynamics are derived from fundamental circuit laws, and the β-component expressions result from the application of (1) to the corresponding α-component dynamics.

The power controller (PC) consists of two PI controllers with gains k_{PC}^p and k_{PC}^i and two low-pass filters with cut-off frequency $\omega_{\mathrm{c,PC}}$ (for the d and q components). The real- and reactive-power setpoints, p^* and q^*, act as inputs to the power controller and its outputs are current references for the downstream current controller. These are generated as follows:

$$i_{\mathrm{i}}^{\mathrm{d}*} = k_{\mathrm{PC}}^p\,(q^* - q_{\mathrm{avg}}) + k_{\mathrm{PC}}^i \int (q^* - q_{\mathrm{avg}})\,, \tag{5a}$$

$$i_{\mathrm{i}}^{\mathrm{q}*} = k_{\mathrm{PC}}^p\,(p^* - p_{\mathrm{avg}}) + k_{\mathrm{PC}}^i \int (p^* - p_{\mathrm{avg}})\,, \tag{5b}$$

where p_{avg} and q_{avg} are the outputs of the low-pass filters, with inputs to be the inverter real- and reactive-power outputs measured at the grid terminals, p and q, respectively. In particular, with reference to Fig. 2 and with the aid of elementary trigonometric operations we have

$$p = \frac{1}{2}(v_{\mathrm{g}}i_{\mathrm{g}}^\alpha + v_{\mathrm{g}}^\beta i_{\mathrm{g}}^\beta), \quad q = \frac{1}{2}(v_{\mathrm{g}}^\beta i_{\mathrm{g}}^\alpha - v_{\mathrm{g}}i_{\mathrm{g}}^\beta), \tag{6}$$

This article has been accepted for publication in a future issue of this journal, but has not been fully edited. Content may change prior to final publication. Citation information: DOI 10.1109/TEC.2018.2881710, IEEE Transactions on Energy Conversion

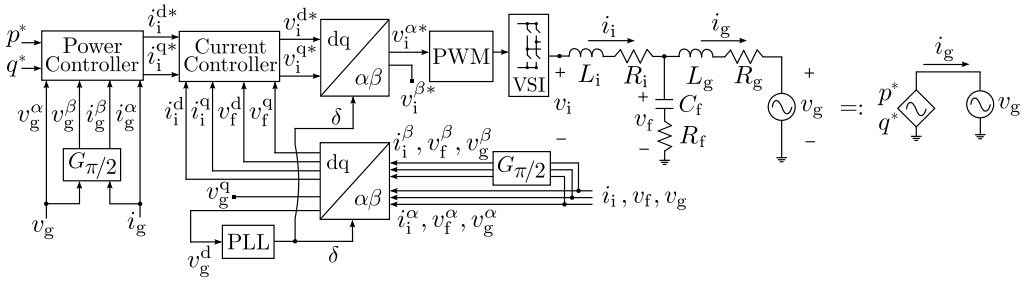

Figure 2: Block diagram of the single-phase inverter and adopted shorthand.

and as discussed above,

$$\frac{d}{dt}p_{\text{avg}} = \omega_{\text{c,PC}}(p - p_{\text{avg}}), \quad \frac{d}{dt}q_{\text{avg}} = \omega_{\text{c,PC}}(q - q_{\text{avg}}). \quad (7)$$

The real-power setpoint, p^*, reflects the real power that is ultimately generated by an upstream input-stage controller and dc-link voltage controller acting in concert. For instance, for a PV application, p^* could be approximated from scaled irradiance data assuming accurate and fast maximum power point tracking. Similarly, the reactive power setpoint, q^*, could either be fixed at zero to reflect unity power factor operation or may alternatively be generated by a Volt/VAR controller. For the sake of generality, we will simply consider p^* and q^* as generic model inputs for the remainder of the paper.

The current controller (CC) is composed of two PI controllers with gains k^p_{CC} and k^i_{CC}, and as outputs, it generates the voltage references for the PWM modulation block:

$$v_{\text{i}}^{\text{d}*} = v_{\text{f}}^{\text{d}} + k^p_{\text{CC}}\left(i_{\text{i}}^{\text{d}*} - i_{\text{i}}^{\text{d}}\right) + k^i_{\text{CC}}\int\left(i_{\text{i}}^{\text{d}*} - i_{\text{i}}^{\text{d}}\right), \quad (8a)$$

$$v_{\text{i}}^{\text{q}*} = v_{\text{f}}^{\text{q}} + k^p_{\text{CC}}\left(i_{\text{i}}^{\text{q}*} - i_{\text{i}}^{\text{q}}\right) + k^i_{\text{CC}}\int\left(i_{\text{i}}^{\text{q}*} - i_{\text{i}}^{\text{q}}\right). \quad (8b)$$

The addition of the feedforward terms v_{f}^{d} and v_{f}^{q} (obtained by applying (2) to v_{f}^{α} and v_{f}^{β}) is standard practice, and intended to improve dynamic performance [30]. Suppose the VSI is ideal (see Fig. 2), then the terminal inverter voltage is given by:

$$v_{\text{i}} \approx v_{\text{i}}^{\alpha*} = v_{\text{i}}^{\text{d}*}\cos\delta - v_{\text{i}}^{\text{q}*}\sin\delta, \quad (9)$$

where δ is the instantaneous PLL angle. This approximation implies that the inverter terminal voltage follows the commanded reference perfectly and without delay.

C. State-space Representation of Inverter Dynamics

The dynamics of the LCL filter, PLL, power controller, and current controller for an individual inverter are now expressed in state-space form to facilitate analysis. To this end, corresponding to the power and current controllers, we will find it useful to introduce the auxiliary dynamics

$$\frac{d}{dt}\phi^{\text{p}} = p^* - p_{\text{avg}}, \quad \frac{d}{dt}\phi^{\text{q}} = q^* - q_{\text{avg}}, \quad (10)$$

$$\frac{d}{dt}\gamma^{\text{d}} = i_{\text{i}}^{\text{d}*} - i_{\text{i}}^{\text{d}}, \quad \frac{d}{dt}\gamma^{\text{q}} = i_{\text{i}}^{\text{q}*} - i_{\text{i}}^{\text{q}}. \quad (11)$$

With these definitions in place, the dynamics (3a)–(11) can be represented in a compact state-space form

$$\dot{x} = Ax + B_1u_1 + B_2u_2 + g(x, u_1, u_2), \quad (12)$$

where the state vector, x, and inputs u_1, u_2 are given by

$$x = [i_{\text{i}}^{\alpha}, i_{\text{i}}^{\beta}, i_{\text{g}}^{\alpha}, i_{\text{g}}^{\beta}, v_{\text{f}}^{\alpha}, v_{\text{f}}^{\beta}, \gamma^{\text{d}}, \gamma^{\text{q}}, p_{\text{avg}}, q_{\text{avg}}, \phi^{\text{p}}, \phi^{\text{q}}, v_{\text{g}}^{\beta}, v_{\text{PLL}}, \phi_{\text{PPL}}, \delta]^{\text{T}}, \quad (13)$$

$$u_1 = [p^*, q^*]^{\text{T}}, \quad u_2 = [v_{\text{g}}, \frac{d}{dt}v_{\text{g}}]^{\text{T}}. \quad (14)$$

In order to show the entries of matrices $A \in \mathbb{R}^{16\times16}$, $B_1 \in \mathbb{R}^{16\times2}$, and $B_2 \in \mathbb{R}^{16\times2}$, let us partition the state vector as $x = [x_{LCL}^{\text{T}}, x_{\text{CC}}^{\text{T}}, x_{\text{PC}}^{\text{T}}, x_{\text{PLL}}^{\text{T}}]^{\text{T}}$, where $x_{LCL} = [i_{\text{i}}^{\alpha}, i_{\text{i}}^{\beta}, i_{\text{g}}^{\alpha}, i_{\text{g}}^{\beta}, v_{\text{f}}^{\alpha}, v_{\text{f}}^{\beta}]^{\text{T}}$, $x_{\text{CC}} = [\gamma^{\text{d}}, \gamma^{\text{q}}]^{\text{T}}$, $x_{\text{PC}} = [p_{\text{avg}}, q_{\text{avg}}, \phi^{\text{p}}, \phi^{\text{q}}]^{\text{T}}$, and $x_{\text{PLL}} = [v_{\text{g}}^{\beta}, v_{\text{PLL}}, \phi_{\text{PLL}}, \delta]^{\text{T}}$. Then, we can write (12) as

$$\begin{bmatrix}\dot{x}_{LCL}\\ \dot{x}_{\text{CC}}\\ \dot{x}_{\text{PC}}\\ \dot{x}_{\text{PLL}}\end{bmatrix} = \begin{bmatrix}A_{LCL} & 0_{6\times2} & 0_{6\times4} & 0_{6\times4}\\ 0_{2\times6} & 0_{2\times2} & A_{\text{CC}} & 0_{2\times4}\\ 0_{4\times6} & 0_{4\times2} & A_{\text{PC}} & 0_{4\times4}\\ 0_{4\times6} & 0_{4\times2} & 0_{4\times4} & A_{\text{PLL}}\end{bmatrix}\begin{bmatrix}x_{LCL}\\ x_{\text{CC}}\\ x_{\text{PC}}\\ x_{\text{PLL}}\end{bmatrix} + \begin{bmatrix}0_{6\times2}\\ B_{\text{CC}}\\ B_{\text{PC}}\\ 0_{4\times2}\end{bmatrix}u_1 + \begin{bmatrix}B_{LCL}\\ 0_{2\times2}\\ 0_{4\times2}\\ B_{\text{PLL}}\end{bmatrix}u_2 + g(x, u_1, u_2), \quad (15)$$

where entries of the nonzero sub-matrices A_{LCL}, A_{CC}, A_{PC}, A_{PLL}, B_{CC}, B_{PC}, B_{LCL}, B_{PLL}, and the function $g(x, u_1, u_2) : \mathbb{R}^{16} \times \mathbb{R}^2 \times \mathbb{R}^2 \to \mathbb{R}^{16}$ are spelled out in Appendix B.

III. Aggregation of Parallel-connected Inverters

In this section, we first introduce parametric scalings required to realize the aggregate model for the parallel-connected inverters. Next, we prove that the aggregate model indeed captures all the scalings in pertinent states (currents, voltages, internal-control states) for the uniform setting as well as in cases with heterogeneous power setpoints and ratings.

A. Parametric Scalings and Structure of Aggregate Model

We consider N identical single-phase inverters (with model described in Section II) with the same setpoints, p^* and q^*, connected in parallel to a grid bus. We are interested in an aggregated reduced-order model with the same structure and dimension as the model in (12):

$$\dot{x}^{\text{r}} = A^{\text{r}}x^{\text{r}} + B_1^{\text{r}}u_1^{\text{r}} + B_2^{\text{r}}u_2^{\text{r}} + g^{\text{r}}(x^{\text{r}}, u_1^{\text{r}}, u_2^{\text{r}}). \quad (16)$$

In particular: we desire matrices $A^{\text{r}} \in \mathbb{R}^{16\times16}$, $B_1^{\text{r}} \in \mathbb{R}^{16\times2}$, $B_2^{\text{r}} \in \mathbb{R}^{16\times2}$, and function $g^{\text{r}} : \mathbb{R}^{16} \times \mathbb{R}^2 \times \mathbb{R}^2 \to \mathbb{R}^{16}$

This article has been accepted for publication in a future issue of this journal, but has not been fully edited. Content may change prior to final publication. Citation information: DOI 10.1109/TEC.2018.2881710, IEEE Transactions on Energy Conversion

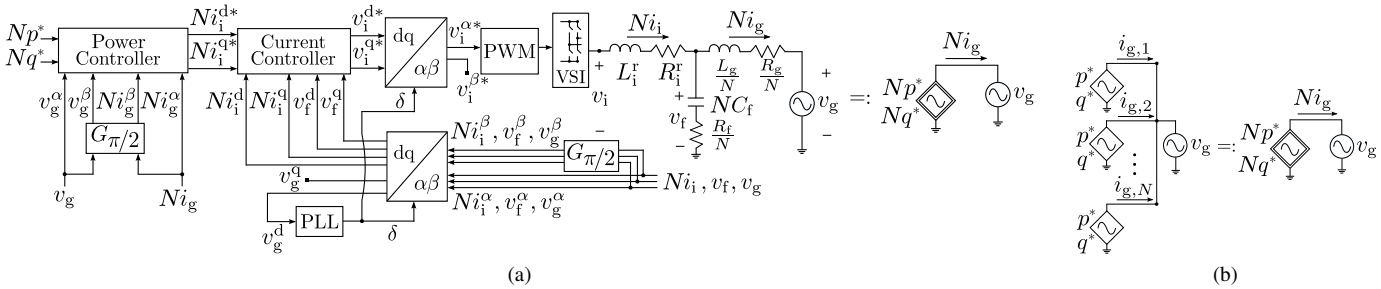

Figure 3: (a) Reduced-order aggregate single-phase inverter model and adopted shorthand representation. The inverter-side inductance and resistance are related to those in the individual model as $\frac{R_{\rm i}^{\rm r}}{L_{\rm i}^{\rm r}} = \frac{R_{\rm i}}{L_{\rm i}}$. (b) Dynamics of the parallel connection of N single-phase inverters can be captured by the aggregate inverter model in Fig. 3a.

have the same structure and dimension as A, B_1, B_2, and g in (12) (implying that the control architecture and output-filter arrangement of the aggregated model are the same as that in an individual inverter); entries of state vector $x^{\rm r}$ and inputs $u_1^{\rm r}$, $u_2^{\rm r}$ to have the same connotation as states in x and inputs u_1, u_2. In our main result, we demonstrate that *if and only if* the following relationships hold between parameters of the reduced-order and original models:

$$C_{\rm f}^{\rm r} = NC_{\rm f},\ R_{\rm f}^{\rm r} = \frac{R_{\rm f}}{N},\ L_{\rm g}^{\rm r} = \frac{L_{\rm g}}{N},\ R_{\rm g}^{\rm r} = \frac{R_{\rm g}}{N}, \tag{17a}$$

$$\frac{R_{\rm i}^{\rm r}}{L_{\rm i}^{\rm r}} = \frac{R_{\rm i}}{L_{\rm i}},\ \frac{k_{\rm CC}^{p,{\rm r}}}{L_{\rm i}^{\rm r}} = \frac{k_{\rm CC}^{p}}{L_{\rm i}},\ \frac{k_{\rm CC}^{i,{\rm r}}}{L_{\rm i}^{\rm r}} = \frac{k_{\rm CC}^{i}}{L_{\rm i}}, \tag{17b}$$

and the reference power settings of the lumped-parameter aggregate inverter model in Fig. 3a are N times those of the inverter model in Fig. 2, the current- and power-related states $i_{\rm i}^{\alpha,{\rm r}}, i_{\rm i}^{\beta,{\rm r}}, i_{\rm f}^{\alpha,{\rm r}}, i_{\rm f}^{\beta,{\rm r}}, \gamma^{{\rm d},{\rm r}}, \gamma^{{\rm q},{\rm r}}, p_{\rm avg}^{\rm r}, q_{\rm avg}^{\rm r}, \phi^{{\rm p},{\rm r}}, \phi^{{\rm q},{\rm r}}$ in the reduced-order model are N times the corresponding ones in an individual inverter. Furthermore, the voltage- and PLL-related states in the reduced-order model $v_{\rm f}^{\alpha,{\rm r}}, v_{\rm f}^{\beta,{\rm r}}, v_{\rm g}^{\beta,{\rm r}}, v_{\rm PLL}^{\rm r}, \phi_{\rm PPL}^{\rm r}, \delta^{\rm r}$ are the same as those in any inverter in the parallel combination. This is consistent with the electrical behavior of a parallel connection of current (or power) sources.

In establishing the above result, we will have established that the reduced-order aggregate model in Fig. 3a captures the dynamics of the parallel collection. Put differently, we will mathematically establish the equivalence illustrated in Fig. 3b. It is worth emphasizing that the dynamical model of an individual inverter has 16 states, and so modeling the dynamics of every inverter in an N-inverter parallel collection would require a $16N$-order state-space model. By contrast, the reduced-order model has the same structure as any individual inverter, and is hence described only by 16 states.

B. Main Result: Validating the Aggregate Model

We now state and prove the main result of this paper.

Theorem 1. (*Aggregation of parallel-connected identical single-phase inverters*) Consider the dynamical model for the single-phase inverter specified in (12). Permute x in (13) as

$$\widehat{x} = [i_{\rm i}^{\alpha}, i_{\rm i}^{\beta}, i_{\rm g}^{\alpha}, i_{\rm g}^{\beta}, \gamma^{\rm d}, \gamma^{\rm q}, p_{\rm avg}, q_{\rm avg}, \phi^{\rm p}, \phi^{\rm q}, v_{\rm f}^{\alpha}, v_{\rm f}^{\beta}, v_{\rm g}^{\beta}, v_{\rm PLL}, \phi_{\rm PPL}, \delta]^{\rm T}, \tag{18}$$

and also permute $x^{\rm r}$ (corresponding to the reduced-order model (16)) the same way, denoting the permuted vector by $\widehat{x}^{\rm r}$. Denote $\widehat{x}(t)$ to be the solution to the permuted version of (12) with initial condition $\widehat{x}(t_0)$ and inputs u_1, u_2; and $\widehat{x}^{\rm r}(t)$ to be the solution to the permuted version of (16) with initial condition $\widehat{x}^{\rm r}(t_0)$ and inputs $u_1^{\rm r}, u_2^{\rm r}$. Suppose initial conditions are such that $\widehat{x}^{\rm r}(t_0) = {\rm diag}(\Psi)\widehat{x}(t_0)$, where the *scaling vector*, $\Psi := [N1_{10}^{\rm T}, 1_6^{\rm T}]^{\rm T}$, and the inputs are: $u_1^{\rm r} = Nu_1, u_2^{\rm r} = u_2$ (see (14)). The states of the reduced-order model and the individual inverter are related as:

$$\widehat{x}^{\rm r}(t) = {\rm diag}(\Psi)\widehat{x}(t), \quad \forall t \geq t_0, \tag{19}$$

if and only if their parameters are related as (17a)–(17b).

In particular, given the definition of the scaling vector, Ψ, (19) establishes the following relationships between states of the reduced-order model and those in the individual inverter model $\forall t \geq t_0$:

$$\begin{aligned}[i_{\rm i}^{\alpha,{\rm r}}, i_{\rm i}^{\beta,{\rm r}}, i_{\rm g}^{\alpha,{\rm r}}, i_{\rm g}^{\beta,{\rm r}}, \gamma^{{\rm d},{\rm r}}, \gamma^{{\rm q},{\rm r}}, p_{\rm avg}^{\rm r}, q_{\rm avg}^{\rm r}, \phi^{{\rm p},{\rm r}}, \phi^{{\rm q},{\rm r}}]^{\rm T} \\ = N[i_{\rm i}^{\alpha}, i_{\rm i}^{\beta}, i_{\rm g}^{\alpha}, i_{\rm g}^{\beta}, \gamma^{\rm d}, \gamma^{\rm q}, p_{\rm avg}, q_{\rm avg}, \phi^{\rm p}, \phi^{\rm q}]^{\rm T},\end{aligned} \tag{20a}$$

$$\begin{aligned}[v_{\rm f}^{\alpha,{\rm r}}, v_{\rm f}^{\beta,{\rm r}}, v_{\rm g}^{\beta,{\rm r}}, v_{\rm PLL}^{\rm r}, \phi_{\rm PPL}^{\rm r}, \delta^{\rm r}]^{\rm T} \\ = [v_{\rm f}^{\alpha}, v_{\rm f}^{\beta}, v_{\rm g}^{\beta}, v_{\rm PLL}, \phi_{\rm PPL}, \delta]^{\rm T}.\end{aligned} \tag{20b}$$

Proof. Let us define $z := \widehat{x}^{\rm r} - {\rm diag}(\Psi)\widehat{x}$. The dynamics of z are given by

$$\begin{aligned}\dot{z} = \dot{\widehat{x}}^{\rm r} - {\rm diag}(\Psi)\dot{\widehat{x}} &= \widehat{A}^{\rm r}\widehat{x}^{\rm r} + \widehat{B}_1^{\rm r}u_1^{\rm r} + \widehat{B}_2^{\rm r}u_2^{\rm r} + \widehat{g}(\widehat{x}^{\rm r}, u_1^{\rm r}, u_2^{\rm r}) \\ &\quad - {\rm diag}(\Psi)\widehat{A}\widehat{x} - {\rm diag}(\Psi)\widehat{B}_1u_1 - {\rm diag}(\Psi)\widehat{B}_2u_2 \\ &\quad - {\rm diag}(\Psi)\widehat{g}(\widehat{x}, u_1, u_2),\end{aligned} \tag{21}$$

where matrices $\widehat{A}$, $\widehat{B}_1$, $\widehat{B}_2$, $\widehat{A}^{\rm r}$, $\widehat{B}_1^{\rm r}$, $\widehat{B}_2^{\rm r}$ and functions $\widehat{g}(\widehat{x}, u_1, u_2)$, $\widehat{g}(\widehat{x}^{\rm r}, u_1^{\rm r}, u_2^{\rm r})$ are appropriately permuted versions of corresponding matrices and functions in (12) and (16). We will now show that $\dot{z} = 0, \forall t \geq t_0$ when $z(t_0) = \widehat{x}^{\rm r}(t_0) - {\rm diag}(\Psi)\widehat{x}(t_0) = 0_{16}$. This would further imply that $z(t) = \widehat{x}^{\rm r}(t) - {\rm diag}(\Psi)\widehat{x}(t) = 0_{16}\ \forall t \geq t_0$, as claimed in the statement of the Theorem.

Partition $\widehat{x} = [\widehat{x}_1^{\rm T}, \widehat{x}_2^{\rm T}]^{\rm T}$, where $\widehat{x}_1 = [i_{\rm i}^{\alpha}, i_{\rm i}^{\beta}, i_{\rm g}^{\alpha}, i_{\rm g}^{\beta}, \gamma^{\rm d}, \gamma^{\rm q}, p_{\rm avg}, q_{\rm avg}, \phi^{\rm p}, \phi^{\rm q}]^{\rm T}$ and $\widehat{x}_2 = [v_{\rm f}^{\alpha}, v_{\rm f}^{\beta}, v_{\rm g}^{\beta}, v_{\rm PLL}, \phi_{\rm PPL}, \delta]^{\rm T}$, and we also partition $\widehat{x}^{\rm r}$ the same way. Then, we partition the appropriately permuted versions of (12) and (16) as

$$\begin{bmatrix}\dot{\widehat{x}}_1 \\ \dot{\widehat{x}}_2\end{bmatrix} = \begin{bmatrix}\widehat{A}_{11} & \widehat{A}_{12} \\ \widehat{A}_{21} & \widehat{A}_{22}\end{bmatrix}\begin{bmatrix}\widehat{x}_1 \\ \widehat{x}_2\end{bmatrix} + \begin{bmatrix}\widehat{B}_{11} \\ \widehat{B}_{12}\end{bmatrix}u_1 + \begin{bmatrix}\widehat{B}_{21} \\ \widehat{B}_{22}\end{bmatrix}u_2$$

This article has been accepted for publication in a future issue of this journal, but has not been fully edited. Content may change prior to final publication. Citation information: DOI 10.1109/TEC.2018.2881710, IEEE Transactions on Energy Conversion

$$+\widehat{g}(\widehat{x},u_1,u_2), \tag{22}$$

$$\begin{bmatrix}\dot{\widehat{x}}_1^{\mathrm{r}}\\ \dot{\widehat{x}}_2^{\mathrm{r}}\end{bmatrix}=\begin{bmatrix}\widehat{A}_{11}^{\mathrm{r}} & \widehat{A}_{12}^{\mathrm{r}}\\ \widehat{A}_{21}^{\mathrm{r}} & \widehat{A}_{22}^{\mathrm{r}}\end{bmatrix}\begin{bmatrix}\widehat{x}_1^{\mathrm{r}}\\ \widehat{x}_2^{\mathrm{r}}\end{bmatrix}+\begin{bmatrix}\widehat{B}_{11}^{\mathrm{r}}\\ \widehat{B}_{12}^{\mathrm{r}}\end{bmatrix}u_1^{\mathrm{r}}+\begin{bmatrix}\widehat{B}_{21}^{\mathrm{r}}\\ \widehat{B}_{22}^{\mathrm{r}}\end{bmatrix}u_2^{\mathrm{r}} +\widehat{g}^{\mathrm{r}}(\widehat{x}^{\mathrm{r}},u_1^{\mathrm{r}},u_2^{\mathrm{r}}). \tag{23}$$

From the definition of matrices A_{LCL}, A_{CC}, A_{PC}, A_{PLL}, B_{CC}, B_{PC}, B_{LCL}, B_{PLL} in Appendix B, and the parametric scalings established in (17a)–(17b), we note the following:

$$\begin{aligned}&\widehat{A}_{11}^{\mathrm{r}}=\widehat{A}_{11},\ \widehat{A}_{12}^{\mathrm{r}}=N\widehat{A}_{12},\ \widehat{A}_{21}^{\mathrm{r}}=\frac{1}{N}\widehat{A}_{21},\ \widehat{A}_{22}^{\mathrm{r}}=\widehat{A}_{22},\\ &\widehat{B}_{11}^{\mathrm{r}}=\widehat{B}_{11},\ \widehat{B}_{12}^{\mathrm{r}}=\frac{1}{N}\widehat{B}_{12},\ \widehat{B}_{21}^{\mathrm{r}}=N\widehat{B}_{21},\ \widehat{B}_{22}^{\mathrm{r}}=\widehat{B}_{22}.\end{aligned} \tag{24}$$

Then, we have

$$\begin{aligned}\mathrm{diag}(\Psi)\widehat{A}&=\begin{bmatrix}N\widehat{A}_{11} & N\widehat{A}_{12}\\ \widehat{A}_{21} & \widehat{A}_{22}\end{bmatrix}=\begin{bmatrix}N\widehat{A}_{11}^{\mathrm{r}} & \widehat{A}_{12}^{\mathrm{r}}\\ N\widehat{A}_{21}^{\mathrm{r}} & \widehat{A}_{22}^{\mathrm{r}}\end{bmatrix}\\ &=\widehat{A}^{\mathrm{r}}\mathrm{diag}(\Psi),\end{aligned} \tag{25}$$

$$\mathrm{diag}(\Psi)\widehat{B}_1=\begin{bmatrix}N\widehat{B}_{11}\\ \widehat{B}_{12}\end{bmatrix}=\begin{bmatrix}N\widehat{B}_{11}^{\mathrm{r}}\\ N\widehat{B}_{12}^{\mathrm{r}}\end{bmatrix}=N\widehat{B}_1^{\mathrm{r}}, \tag{26}$$

$$\mathrm{diag}(\Psi)\widehat{B}_2=\begin{bmatrix}N\widehat{B}_{21}\\ \widehat{B}_{22}\end{bmatrix}=\begin{bmatrix}\widehat{B}_{21}^{\mathrm{r}}\\ \widehat{B}_{22}^{\mathrm{r}}\end{bmatrix}=\widehat{B}_2^{\mathrm{r}}. \tag{27}$$

The next step is to show that $\widehat{g}^{\mathrm{r}}(\mathrm{diag}(\Psi)\widehat{x},u_1^{\mathrm{r}},u_2^{\mathrm{r}})=\mathrm{diag}(\Psi)\widehat{g}(\widehat{x},u_1,u_2)$. Let $\widehat{g}_\ell(\widehat{x})$ and $\widehat{g}_\ell^{\mathrm{r}}(\mathrm{diag}(\Psi)\widehat{x})$ denote the ℓ-th entry of $\widehat{g}(\widehat{x},u_1,u_2)$ and $\widehat{g}^{\mathrm{r}}(\mathrm{diag}(\Psi)\widehat{x},u_1^{\mathrm{r}},u_2^{\mathrm{r}})$, respectively. The nonzero entries of $\widehat{g}^{\mathrm{r}}(\mathrm{diag}(\Psi)\widehat{x},u_1^{\mathrm{r}},u_2^{\mathrm{r}})$ are related to the corresponding entries of $\widehat{g}(\widehat{x},u_1,u_2)$ through:

$$\begin{aligned}&\widehat{g}_1^{\mathrm{r}}(\mathrm{diag}(\Psi)\widehat{x})=\frac{N}{L_{\mathrm{i}}}\Bigg[\Bigg(\frac{k_{\mathrm{CC}}^p}{N}\left(k_{\mathrm{PC}}^p(Nq^*-Nq_{\mathrm{avg}})+k_{\mathrm{PC}}^iN\phi^{\mathrm{q}}\right.\\ &\left.-Ni_{\mathrm{i}}^{\mathrm{d}}\right)+\frac{k_{\mathrm{CC}}^i}{N}N\gamma^{\mathrm{d}}\Bigg)\cos\delta-\Bigg(\frac{k_{\mathrm{CC}}^p}{N}\left(k_{\mathrm{PC}}^p(Np^*-Np_{\mathrm{avg}})\right.\\ &\left.+k_{\mathrm{PC}}^iN\phi^{\mathrm{p}}-Ni_{\mathrm{i}}^{\mathrm{q}}\right)+\frac{k_{\mathrm{CC}}^i}{N}N\gamma^{\mathrm{q}}\Bigg)\sin\delta\Bigg]=N\widehat{g}_1(\widehat{x}),\\ &\widehat{g}_2^{\mathrm{r}}(\mathrm{diag}(\Psi)\widehat{x})=\eta(Ni_{\mathrm{i}}^\alpha-Ni_{\mathrm{i}}^\beta)-\widehat{g}_1^{\mathrm{r}}(\mathrm{diag}(\Psi)\widehat{x})=N\widehat{g}_2(\widehat{x}),\\ &\widehat{g}_5^{\mathrm{r}}(\mathrm{diag}(\Psi)\widehat{x})=-Ni_{\mathrm{i}}^\alpha\cos\delta-Ni_{\mathrm{i}}^\beta\sin\delta=N\widehat{g}_5(\widehat{x}),\\ &\widehat{g}_6^{\mathrm{r}}(\mathrm{diag}(\Psi)\widehat{x})=Ni_{\mathrm{i}}^\alpha\sin\delta-Ni_{\mathrm{i}}^\beta\cos\delta=N\widehat{g}_6(\widehat{x}),\\ &\widehat{g}_7^{\mathrm{r}}(\mathrm{diag}(\Psi)\widehat{x})=\frac{\omega_{\mathrm{c,PC}}}{2}(v_{\mathrm{g}}Ni_{\mathrm{g}}^\alpha+v_{\mathrm{g}}^\beta Ni_{\mathrm{g}}^\beta)=N\widehat{g}_7(\widehat{x}),\\ &\widehat{g}_8^{\mathrm{r}}(\mathrm{diag}(\Psi)\widehat{x})=\frac{\omega_{\mathrm{c,PC}}}{2}(v_{\mathrm{g}}^\beta Ni_{\mathrm{g}}^\alpha-v_{\mathrm{g}}Ni_{\mathrm{g}}^\beta)=N\widehat{g}_8(\widehat{x}),\\ &\widehat{g}_{11}^{\mathrm{r}}(\mathrm{diag}(\Psi)\widehat{x})=\frac{R_{\mathrm{f}}}{N}\widehat{g}_1^{\mathrm{r}}(\mathrm{diag}(\Psi)\widehat{x})=R_{\mathrm{f}}\widehat{g}_1(\widehat{x})=\widehat{g}_{11}(\widehat{x}),\\ &\widehat{g}_{12}^{\mathrm{r}}(\mathrm{diag}(\Psi)\widehat{x})=\eta(v_{\mathrm{f}}^\alpha-v_{\mathrm{f}}^\beta)-\widehat{g}_{11}^{\mathrm{r}}(\mathrm{diag}(\Psi)\widehat{x})=\widehat{g}_{12}(\widehat{x}),\\ &\widehat{g}_{13}^{\mathrm{r}}(\mathrm{diag}(\Psi)\widehat{x})=\eta(v_{\mathrm{g}}-v_{\mathrm{g}}^\beta)=\widehat{g}_{13}(\widehat{x}),\\ &\widehat{g}_{14}^{\mathrm{r}}(\mathrm{diag}(\Psi)\widehat{x})=\omega_{\mathrm{c,PLL}}(v_{\mathrm{g}}\cos\delta+v_{\mathrm{g}}^\beta\sin\delta)=\widehat{g}_{14}(\widehat{x}),\\ &\widehat{g}_{16}^{\mathrm{r}}(\mathrm{diag}(\Psi)\widehat{x})=\omega_{\mathrm{nom}}=\widehat{g}_{16}(\widehat{x}),\end{aligned}$$

with $\eta:=-k_{\mathrm{PLL}}^pv_{\mathrm{PLL}}+k_{\mathrm{PLL}}^i\phi_{\mathrm{PLL}}$. Therefore we have

$$\mathrm{diag}(\Psi)\widehat{g}(\widehat{x},u_1,u_2)=\widehat{g}^{\mathrm{r}}(\mathrm{diag}(\Psi)\widehat{x},u_1^{\mathrm{r}},u_2^{\mathrm{r}}). \tag{28}$$

Notice that the PLL dynamics ((3a)–(3d)) are decoupled from the remainder of the states in the state-space model. Therefore, the parameters of the PLL in the individual and reduced-order models are the same, and we can conclude that:

$$v_{\mathrm{g}}^{\beta,\mathrm{r}}=v_{\mathrm{g}}^\beta,\quad v_{\mathrm{PLL}}^{\mathrm{r}}=v_{\mathrm{PLL}},\quad \phi_{\mathrm{PLL}}^{\mathrm{r}}=\phi_{\mathrm{PLL}},\quad \delta^{\mathrm{r}}=\delta. \tag{29}$$

Now, consider the function $h(\widehat{x}^{\mathrm{r}},u_1^{\mathrm{r}},u_2^{\mathrm{r}}):\mathbb{R}^{16}\times\mathbb{R}^2\times\mathbb{R}^2\to\mathbb{R}^{16}$, which is defined to have the same structure as $\widehat{g}^{\mathrm{r}}(\widehat{x}^{\mathrm{r}},u_1^{\mathrm{r}},u_2^{\mathrm{r}})$ except that its 13th, 14th, and 16th entries are 0. (See Appendix B for details.) Then, the following holds

$$\begin{aligned}&\widehat{g}^{\mathrm{r}}(\widehat{x}^{\mathrm{r}},u_1^{\mathrm{r}},u_2^{\mathrm{r}})-\widehat{g}^{\mathrm{r}}(\mathrm{diag}(\Psi)\widehat{x},u_1^{\mathrm{r}},u_2^{\mathrm{r}})\\ &\qquad=h((\widehat{x}^{\mathrm{r}}-\mathrm{diag}\,(\Psi)\widehat{x}),0_2,u_2^{\mathrm{r}}).\end{aligned} \tag{30}$$

Using identities (25)–(30) in (21), we have

$$\begin{aligned}\dot{z}&=\widehat{A}^{\mathrm{r}}(\widehat{x}^{\mathrm{r}}-\mathrm{diag}(\Psi)\widehat{x})+h((\widehat{x}^{\mathrm{r}}-\mathrm{diag}\,(\Psi)\widehat{x}),0_2,u_2^{\mathrm{r}})\\ &=\widehat{A}^{\mathrm{r}}z+h(z,0_2,u_2^{\mathrm{r}}).\end{aligned} \tag{31}$$

If we initialize $z(t_0)=0_{16}$, we have $z(t)=0_{16},\forall t\geq t_0$, due to the fact that $h(0_{16},0_2,u_2^{\mathrm{r}})=0_{16}$. By the definition of $z(t)$, we have $\widehat{x}^{\mathrm{r}}(t)=\mathrm{diag}(\Psi)\widehat{x}(t),\forall t\geq t_0$.

For the other direction, given that $z(t)=\widehat{x}^{\mathrm{r}}-\mathrm{diag}(\Psi)\widehat{x}$, $\forall t\geq t_0$, $u_1^{\mathrm{r}}=Nu_1$, and $u_2^{\mathrm{r}}=u_2$, (21) can be written as

$$\begin{aligned}0_{15}=&(\widehat{A}^{\mathrm{r}}\mathrm{diag}(\Psi)-\mathrm{diag}(\Psi)\widehat{A})\widehat{x}+(N\widehat{B}_1^{\mathrm{r}}-\mathrm{diag}(\Psi)\widehat{B}_1)u_1\\ &+(\widehat{B}_2^{\mathrm{r}}-\mathrm{diag}(\Psi)\widehat{B}_2)u_2+\widehat{g}^{\mathrm{r}}(\mathrm{diag}(\Psi)\widehat{x},Nu_1,u_2)\\ &-\mathrm{diag}(\Psi)\widehat{g}(\widehat{x},u_1,u_2).\end{aligned} \tag{32}$$

The equality above is satisfied when the following identities hold:

$$\begin{aligned}&\widehat{A}^{\mathrm{r}}\mathrm{diag}(\Psi)=\mathrm{diag}(\Psi)\widehat{A},\quad N\widehat{B}_1^{\mathrm{r}}=\mathrm{diag}(\Psi)\widehat{B}_1,\\ &\widehat{B}_2^{\mathrm{r}}=\mathrm{diag}(\Psi)\widehat{B}_2,\end{aligned} \tag{33}$$

$$\widehat{g}^{\mathrm{r}}(\mathrm{diag}(\Psi)\widehat{x},Nu_1,u_2)=\mathrm{diag}(\Psi)\widehat{g}(\widehat{x},u_1,u_2). \tag{34}$$

It emerges that R_{i}, L_{i}, k_{CC}^p, and k_{CC}^i always appear in the identities above as fractions: $\frac{R_{\mathrm{i}}}{L_{\mathrm{i}}}$, $\frac{k_{\mathrm{CC}}^p}{L_{\mathrm{i}}}$, and $\frac{k_{\mathrm{CC}}^i}{L_{\mathrm{i}}}$. Therefore, these parameters relate to those in the reduced-order model through (17b). The remainder of the parameters can be determined straightforwardly from (33) and (34); they are given uniquely by (17a), including the unchanged parameters (i.e., those which are not mentioned in (17a) and (17b)). This concludes the proof. □

C. Corollaries for Heterogeneous Settings

We now present two corollaries. In the first, we examine inverters with different reference-power setpoints for both active and reactive power. In this particular case, the relationships between the states of the reduced-order model and those of the individual inverters $\ell=1,\ldots,N$ are as follows $\forall t\geq t_0$:

$$\begin{aligned}&[i_{\mathrm{i}}^{\alpha,\mathrm{r}},i_{\mathrm{i}}^{\beta,\mathrm{r}},i_{\mathrm{g}}^{\alpha,\mathrm{r}},i_{\mathrm{g}}^{\beta,\mathrm{r}},\gamma^{\mathrm{d,r}},\gamma^{\mathrm{q,r}},p_{\mathrm{avg}}^{\mathrm{r}},q_{\mathrm{avg}}^{\mathrm{r}},\phi^{\mathrm{p,r}},\phi^{\mathrm{q,r}}]^{\mathrm{T}}\\ &=\sum_{\ell=1}^N[i_{\mathrm{i},\ell}^\alpha,i_{\mathrm{i},\ell}^\beta,i_{\mathrm{g},\ell}^\alpha,i_{\mathrm{g},\ell}^\beta,\gamma_\ell^{\mathrm{d}},\gamma_\ell^{\mathrm{q}},p_{\mathrm{avg},\ell},q_{\mathrm{avg},\ell},\phi_\ell^{\mathrm{p}},\phi_\ell^{\mathrm{q}}]^{\mathrm{T}},\\ &[v_{\mathrm{f}}^{\alpha,\mathrm{r}},v_{\mathrm{f}}^{\beta,\mathrm{r}}]^{\mathrm{T}}=\frac{1}{N}\sum_{\ell=1}^N[v_{\mathrm{f},\ell}^\alpha,v_{\mathrm{f},\ell}^\beta]^{\mathrm{T}},\\ &[v_{\mathrm{g}}^{\beta,\mathrm{r}},v_{\mathrm{PLL}}^{\mathrm{r}},\phi_{\mathrm{PPL}}^{\mathrm{r}},\delta^{\mathrm{r}}]^{\mathrm{T}}=[v_{\mathrm{g},\ell}^\beta,v_{\mathrm{PLL},\ell},\phi_{\mathrm{PPL},\ell},\delta_\ell]^{\mathrm{T}},\forall\ell.\end{aligned}$$

This article has been accepted for publication in a future issue of this journal, but has not been fully edited. Content may change prior to final publication. Citation information: DOI 10.1109/TEC.2018.2881710, IEEE Transactions on Energy Conversion

This model is useful in, e.g., PV systems where the incident irradiation might be different for different inverters (hence resulting in different values for p^*) and where local-voltage control may be implemented by modulating reactive-power injections (hence resulting in different values of q^*).

In the second corollary, we examine inverters with different power ratings, and derive an aggregate model with currents that scale systematically. To formalize this, we define a *power-scaling parameter* κ_ℓ for the ℓ-th inverter as [26]:

$$\kappa_\ell = \frac{p_{\text{rated},\ell}}{p_{\text{base}}}, \tag{36}$$

where $p_{\text{rated},\ell}$ and p_{base} denote the rated power of the ℓ-th inverter in the parallel system and system-wide base value, respectively. Without loss of generality, we assume that the inverter model in Fig. 2 has a power rating equal to the base value. We also introduce the notion of an *equivalent power-scaling parameter*:

$$\overline{\kappa} := \sum_{\ell=1}^{N} \kappa_\ell. \tag{37}$$

The states of the reduced-order model relate to those in the individual inverters $\ell = 1, \ldots, N$ and the *unscaled* inverter (i.e., inverter model with rating equal to the base value) as follows $\forall t \geq t_0$:

$$\begin{aligned}
&[i_{\text{i}}^{\alpha,\text{r}}, i_{\text{i}}^{\beta,\text{r}}, i_{\text{g}}^{\alpha,\text{r}}, i_{\text{g}}^{\beta,\text{r}}, \gamma^{\text{d},\text{r}}, \gamma^{\text{q},\text{r}}, p_{\text{avg}}^{\text{r}}, q_{\text{avg}}^{\text{r}}, \phi^{\text{p},\text{r}}, \phi^{\text{q},\text{r}}]^{\text{T}} \\
&= \sum_{\ell=1}^{N} [i_{\text{i},\ell}^{\alpha}, i_{\text{i},\ell}^{\beta}, i_{\text{g},\ell}^{\alpha}, i_{\text{g},\ell}^{\beta}, \gamma_\ell^{\text{d}}, \gamma_\ell^{\text{q}}, p_{\text{avg},\ell}, q_{\text{avg},\ell}, \phi_\ell^{\text{p}}, \phi_\ell^{\text{q}}]^{\text{T}} \\
&= \overline{\kappa}[i_{\text{i}}^{\alpha}, i_{\text{i}}^{\beta}, i_{\text{g}}^{\alpha}, i_{\text{g}}^{\beta}, \gamma^{\text{d}}, \gamma^{\text{q}}, p_{\text{avg}}, q_{\text{avg}}, \phi^{\text{p}}, \phi^{\text{q}}]^{\text{T}}, \\
&[v_{\text{f}}^{\alpha,\text{r}}, v_{\text{f}}^{\beta,\text{r}}, v_{\text{g}}^{\beta,\text{r}}, v_{\text{PLL}}^{\text{r}}, \phi_{\text{PPL}}^{\text{r}}, \delta^{\text{r}}]^{\text{T}} \\
&= [v_{\text{f},\ell}^{\alpha}, v_{\text{f},\ell}^{\beta}, v_{\text{g},\ell}^{\beta}, v_{\text{PLL},\ell}, \phi_{\text{PPL},\ell}, \delta_\ell]^{\text{T}}, \forall \ell \\
&= [v_{\text{f}}^{\alpha}, v_{\text{f}}^{\beta}, v_{\text{g}}^{\beta}, v_{\text{PLL}} \phi_{\text{PPL}}, \delta]^{\text{T}}.
\end{aligned}$$

Formal results establishing these two aspects follow next.

Corollary 1. (*Aggregation of parallel-connected identical single-phase inverters with different reference-power setpoints*) Let us denote x_ℓ, p_ℓ^*, and q_ℓ^* as the state vector, real-, and reactive-power setpoints of the ℓ-th inverter in the parallel system. Permute x_ℓ the same way as in (18), denoting the permuted vector as $\widehat{x}_\ell$. Partition $\widehat{x}_\ell = [\lambda_\ell^{\text{T}}, v_{\text{f},\ell}^{\alpha\beta\text{T}}, x_{\text{PLL},\ell}^{\text{T}}]^{\text{T}}$, where $\lambda_\ell = [i_{\text{i},\ell}^{\alpha}, i_{\text{i},\ell}^{\beta}, i_{\text{g},\ell}^{\alpha}, i_{\text{g},\ell}^{\beta}, \gamma_\ell^{\text{d}}, \gamma_\ell^{\text{q}}, p_{\text{avg},\ell}, q_{\text{avg},\ell}, \phi_\ell^{\text{p}}, \phi_\ell^{\text{q}}]^{\text{T}}$, $v_{\text{f},\ell}^{\alpha\beta} = [v_{\text{f},\ell}^{\alpha}, v_{\text{f},\ell}^{\beta}]^{\text{T}}$, and $x_{\text{PLL}} = [v_{\text{g},\ell}^{\beta}, v_{\text{PLL},\ell}, \phi_{\text{PPL},\ell}, \delta_\ell]^{\text{T}}$. We also permute and partition x^{r} the same way, denoting the permuted vector as $\widehat{x}^{\text{r}} = [\lambda^{\text{r}\text{T}}, v_{\text{f}}^{\alpha\beta,\text{r}\text{T}}, x_{\text{PLL}}^{\text{r}\text{T}}]^{\text{T}}$. Suppose the initial conditions are such that $\lambda^{\text{r}}(t_0) = \sum_{\ell=1}^{N} \lambda_\ell(t_0)$, $v_{\text{f}}^{\alpha\beta,\text{r}}(t_0) = \frac{1}{N}\sum_{\ell=1}^{N} v_{\text{f},\ell}^{\alpha\beta}(t_0)$, and $x_{\text{PLL}}^{\text{r}}(t_0) = x_{\text{PLL},\ell}(t_0), \forall \ell$, and the inputs are:

$$u_1^{\text{r}} = \sum_{\ell=1}^{N} u_{1,\ell}, \quad u_2^{\text{r}} = u_2. \tag{39}$$

It follows that, $\forall t \geq t_0$:

$$\begin{gathered}
\lambda^{\text{r}}(t) = \sum_{\ell=1}^{N} \lambda_\ell(t), \quad v_{\text{f}}^{\alpha\beta,\text{r}}(t) = \frac{1}{N}\sum_{\ell=1}^{N} v_{\text{f},\ell}^{\alpha\beta}(t), \\
x_{\text{PLL}}^{\text{r}}(t) = x_{\text{PLL},\ell}(t), \forall \ell,
\end{gathered} \tag{40}$$

if and only if the parameters of the reduced-order are related to the individual inverters through (17a)–(17b).

Proof. The proof is provided in Appendix C. □

Corollary 2. (*Aggregation of parallel-connected single-phase inverters with heterogeneous power ratings*) The parameters of each inverter are related to the unscaled inverter through

$$C_{\text{f},\ell} = \kappa_\ell C_{\text{f}},\ R_{\text{f},\ell} = \frac{R_{\text{f}}}{\kappa_\ell},\ L_{\text{g},\ell} = \frac{L_{\text{g}}}{\kappa_\ell},\ R_{\text{g},\ell} = \frac{R_{\text{g}}}{\kappa_\ell}, \tag{41a}$$

$$\frac{R_{\text{i},\ell}}{L_{\text{i},\ell}} = \frac{R_{\text{i}}}{L_{\text{i}}},\ \frac{k_{\text{CC},\ell}^{p}}{L_{\text{i},\ell}} = \frac{k_{\text{CC}}^{p}}{L_{\text{i}}},\ \frac{k_{\text{CC},\ell}^{i}}{L_{\text{i},\ell}} = \frac{k_{\text{CC}}^{i}}{L_{\text{i}}}, \tag{41b}$$

and parameters not mentioned are unchanged. Suppose the reference-power setpoints for each inverter are $p_\ell^* = \kappa_\ell p^*$ and $q_\ell^* = \kappa_\ell q^*$. The parameters of the reduced-order model are related to the unscaled inverter through

$$C_{\text{f}}^{\text{r}} = \overline{\kappa} C_{\text{f}},\ R_{\text{f}}^{\text{r}} = \frac{R_{\text{f}}}{\overline{\kappa}},\ L_{\text{g}}^{\text{r}} = \frac{L_{\text{g}}}{\overline{\kappa}},\ R_{\text{g}}^{\text{r}} = \frac{R_{\text{g}}}{\overline{\kappa}}, \tag{42a}$$

$$\frac{R_{\text{i}}^{\text{r}}}{L_{\text{i}}^{\text{r}}} = \frac{R_{\text{i}}}{L_{\text{i}}},\ \frac{k_{\text{CC}}^{p,\text{r}}}{L_{\text{i}}^{\text{r}}} = \frac{k_{\text{CC}}^{p}}{L_{\text{i}}},\ \frac{k_{\text{CC}}^{i,\text{r}}}{L_{\text{i}}^{\text{r}}} = \frac{k_{\text{CC}}^{i}}{L_{\text{i}}}. \tag{42b}$$

Parameters not mentioned are unchanged. Let x, x_ℓ, x^{r} denote the state vectors of the unscaled inverter model, ℓ-th inverter of the parallel system, and the reduced-order model, respectively. Permute the state vectors the same way as (18), denoting the permuted vectors as $\widehat{x}$, $\widehat{x}_\ell$, $\widehat{x}^{\text{r}}$. Partition the permuted state vector $\widehat{x} = [\lambda^{\text{T}}, \psi^{\text{T}}]^{\text{T}}$, where $\lambda = [i_{\text{i}}^{\alpha}, i_{\text{i}}^{\beta}, i_{\text{g}}^{\alpha}, i_{\text{g}}^{\beta}, \gamma^{\text{d}}, \gamma^{\text{q}}, p_{\text{avg}}, q_{\text{avg}}, \phi^{\text{p}}, \phi^{\text{q}}]^{\text{T}}$ and $\psi = [v_{\text{f}}^{\alpha}, v_{\text{f}}^{\beta}, v_{\text{g}}^{\beta}, v_{\text{PLL}}, \phi_{\text{PLL}}, \delta]^{\text{T}}$. We also partition $\widehat{x}_\ell$ and $\widehat{x}^{\text{r}}$ the same way: $\widehat{x}_\ell = [\lambda_\ell^{\text{T}}, \psi_\ell^{\text{T}}]^{\text{T}}$, $\widehat{x}^{\text{r}} = [\lambda^{\text{r}\text{T}}, \psi^{\text{r}\text{T}}]^{\text{T}}$. Suppose the initial conditions are such that $\lambda^{\text{r}}(t_0) = \sum_{\ell=1}^{N} \lambda_\ell(t_0) = \overline{\kappa}\lambda(t_0)$, $\psi^{\text{r}}(t_0) = \psi_\ell(t_0) = \psi(t_0), \forall \ell$, and the inputs are:

$$u_1^{\text{r}} = \sum_{\ell=1}^{N} u_{1,\ell} = \overline{\kappa} u_1, \quad u_2^{\text{r}} = u_{2,\ell} = u_2, \forall \ell. \tag{43}$$

It follows that for $t \geq t_0$:

$$\lambda^{\text{r}}(t) = \sum_{\ell=1}^{N} \lambda_\ell(t) = \overline{\kappa}\lambda(t),\ \psi^{\text{r}}(t) = \psi_\ell(t) = \psi(t), \forall \ell, \tag{44}$$

if and only if the parameters of the reduced-order model are related to the unscaled inverter through (42a)–(42b).

Proof. Each of the inverters in the parallel system can be viewed as the aggregate of κ_ℓ inverters, while keeping in mind that κ_ℓ is not necessarily an integer. The rest of this proof is straightforward from Theorem 1. □

IV. Experimental Validation & Simulation Results

In this section, we outline results from an experimental prototype and an exhaustive simulation study to demonstrate various aspects of the reduced-order model. The purpose and scope of the experiments is to demonstrate the validity and establish the accuracy of the reduced-order model (under uniform and symmetric settings) and this is done by comparing the net current injected by the parallel system of inverters in hardware to the output current of the aggregated reduced-order model. The experiments also establish robustness of the

This article has been accepted for publication in a future issue of this journal, but has not been fully edited. Content may change prior to final publication. Citation information: DOI 10.1109/TEC.2018.2881710, IEEE Transactions on Energy Conversion

Table I: Inverter LCL-filter and controller parameters.

LCL filter	Current Controller	PLL
$L_\mathrm{i} = 1.0\,\mathrm{mH}$	$k^p_\mathrm{CC} = 6\,\mathrm{V/A}$	$k^p_\mathrm{PLL} = 1.25\,\mathrm{rad/(V\cdot s)}$
$R_\mathrm{i} = 0.7\,\Omega$	$k^i_\mathrm{CC} = 350\,\mathrm{V/(A\cdot s)}$	$k^i_\mathrm{PLL} = 10\,\mathrm{rad/(V\cdot s^2)}$
$C_\mathrm{f} = 24\,\mu\mathrm{F}$		$\omega_\mathrm{c,PLL} = 2\pi\times 200\,\mathrm{rad/s}$
$R_\mathrm{f} = 0.02\,\Omega$	Power Controller	
$L_\mathrm{g} = 0.2\,\mathrm{mH}$	$k^p_\mathrm{PC} = 0.01\,\mathrm{A/VA}$	
$R_\mathrm{g} = 0.12\,\Omega$	$k^i_\mathrm{PC} = 0.1\,\mathrm{A/(VA\cdot s)}$	
	$\omega_\mathrm{c,PC} = 50.26\,\mathrm{rad/s}$	

reduced-order model to parametric variations that are indeed inescapable in any hardware setup. Following the experimental results, we also include an exhaustive simulation study that: validates the reduced-order model derived for hetereogeneous settings (Corollaries 1 and 2), investigates robustness of the reduced-order model to variations in filter parameters, and demonstrates the computational benefits of the reduced-order model.

A. Hardware Setup

To validate the reduced-order model, we built an experimental system comprised of three identical 750 VA single-phase inverters connected in parallel across a stiff voltage source. The hardware setup is illustrated in Fig. 4(a). It consists of three distinct inverters each with a dedicated power stage and a TI F28335 DSP controller. Each inverter utilizes the control structure shown in Fig. 2. Controllers are discretized with a step size of $1/(15\times 10^3)$ s and unipolar sine-triangle PWM is utilized with a switching frequency of 30 kHz. The single-phase 60 Hz, 120 V RMS ac system voltage (i.e., the grid point of interconnection) is realized with an Ametek MX-45 grid simulator. Subsequently, measurements obtained from the multi-inverter system are compared to a software simulation of a single aggregated inverter model (see Figs. 3a and 4(b)). The simulation of the aggregated inverter, as given in Fig. 4(b), was carried in MATLAB with the ODE45 solver, performed on a computer with Intel Core i7-7700HQ processor @ 2.80GHz CPU and 8GB RAM. The parameters of the experimental setup are summarized in Table I. Simulation parameters used in the aggregated inverter model are obtained from these, and the scalings reported in (17a)–(17b).

B. Validation of Reduced-order Model

To validate the proposed reduced-order model, we compared the measured and simulated dynamic responses under a comprehensive set of step changes in both real and reactive power. The real-power steps are representative of, e.g., sudden irradiance transients that a microinverter system might contend with. The reactive-power steps are representative of, e.g., ancillary services that grid-connected inverters may provide. Results are plotted in Fig. 5. The plot pair in each subfigure illustrates:

1) The measured net sinusoidal current injected into the grid by the parallel inverters overlaid with the simulated current from the aggregated-inverter model. The measurement point and corresponding point in the reduced-order model are marked prominently in Fig. 4.

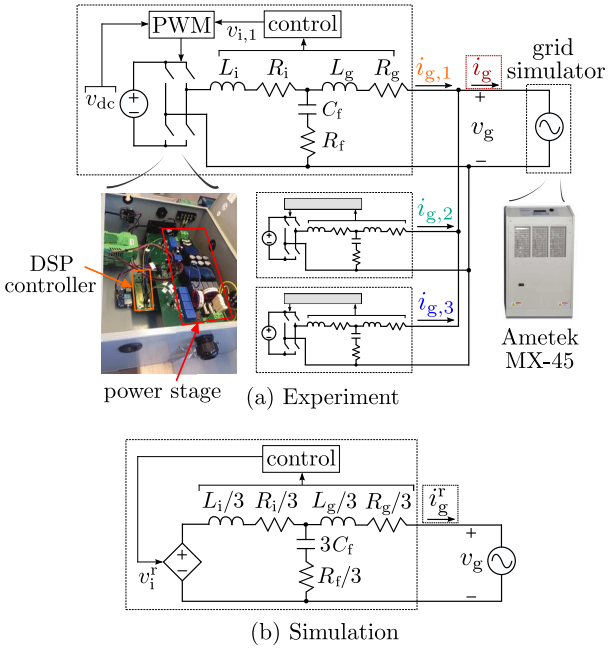

Figure 4: (a) Experimental setup consisting of three parallel-connected single-phase inverters rated at 750 VA. The system of three inverters are given real- and reactive-power step commands to generate the results in Fig. 5 (Currents plotted in Fig. 5 are shown in dashed boxes, marked with the same color scheme above.) (b) The reduced-order aggregated model where the multi-inverter system is represented as one equivalent inverter.

2) Pertinent d- or q-axis current waveforms measured at each inverter output in addition to measured and simulated net current injection.

It is worth emphasizing that we focus just on the *net* current at the point of grid interconnection and compare that with the current suggested by the aggregate model. The match between these through a variety of large-signal changes—as suggested in Fig. 5—validates the accuracy of the aggregate model. Furthermore, note that in this case, the parallel collection of inverters are collectively described by a 48-state model, while the simulations are performed with the reduced-order 16-state model.

C. Simulation Study

Next, we establish the accuracy and computational benefits of the proposed reduced-order model (for a system of 100 parallel-connected inverters) in heterogeneous settings with numerical simulation results. The parameters of the inverter with nominal power rating are listed in Table I. We consider the following cases: #1) Inverters have heterogeneous power ratings with power-scaling parameters κ selected to be uniformly distributed between 0.5 and 5. #2) All inverters have ratings that match the nominal power ratings, but their LCL-filter parameters vary between $\pm 10\%$ of their nominal values. #3) Same setup as #2, but the LCL-filter parameters of the inverters vary between $\pm 80\%$ of their nominal values. For all cases, the real- and reactive-power setpoints of the inverters are assumed to be uniformly distributed between $0-200$ W and $0-100$ VAR, respectively, and we perform a step change

This article has been accepted for publication in a future issue of this journal, but has not been fully edited. Content may change prior to final publication. Citation information: DOI 10.1109/TEC.2018.2881710, IEEE Transactions on Energy Conversion

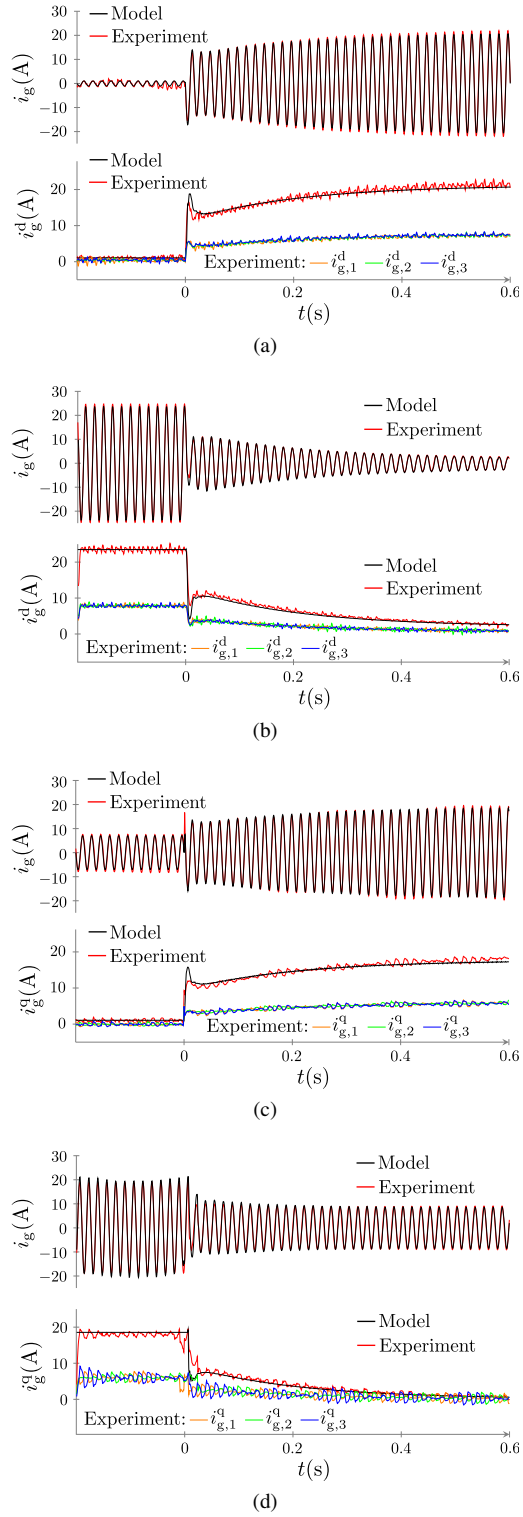

Figure 5: Comparison of experimentally measured and simulated waveforms: (a) Real-power step up p^* : 30 W $\rightarrow$ 600 W with fixed $q^* = 0$ VAR, (b) Real-power step down p^* : 700 W $\rightarrow$ 50 W with fixed $q^* = 0$ VAR, (c) Reactive-power step up q^* : 0 VAR $\rightarrow$ 500 W with fixed $p^* = 200$ W, (d) Reactive-power step down q^* : 500 VAR $\rightarrow$ 0 W with fixed $p^* = 250$ W.

to both setpoints, with the values again selected to be uniformly distributed between $400-600$ W and $300-500$ VAR, respectively. The step change is introduced at $t = 2$ s, and we stop the simulations at $t = 4$ s. We note that case #2 and #3 have the same reduced-order model. The parameter scalings of the reduced-order models for case #1 and #2 (#3) are given by (42a)–(42b) and (17a)–(17b), respectively. The net current injection of the multi-inverter system and the reduced-order models for case #1, #2, and #3 are shown in Fig. 6. We can clearly see in Fig. 6a that for case#1, the output current of the reduced-order model is exactly the same as the net current injection of the parallel system—this validates Corollaries 1 and 2. Furthermore, Fig. 6b shows that the reduced-order model is quite robust with respect to the parametric variations in the LCL filter parameters with discrepancies obvious in high-frequency content. For larger variation ($\pm 80\%$), Fig. 6c shows that the reduced-order model captures the dynamics of the multi-inverter system, albeit with degraded accuracy during the transient. Finally, the computation time for the 1600-th order multi-inverter system simulation for cases #1 and #2 are 58.23 s, 66.97 s, and 145.08 s, respectively, and of the reduced-order 16-th order aggregate model are 1.89 s, 1.62 s, and 1.62 s, respectively. This clearly establishes the computational benefits of the proposed model.

V. Concluding Remarks and Directions for Future Work

In this paper, we derived a reduced-order aggregated model for identical parallel-connected grid-tied single-phase inverters and extensions covering cases when the inverter power-setpoints are different and the inverter power ratings are different. The reduced-order model preserves the structure and has the same order as any individual inverter in the parallel collection. Experimental validation was provided to establish the accuracy of the reduced-order model in capturing ac-side dynamics of inverters during large-signal transients, and simulation results were provided to demonstrate computational benefits and robustness to parametric variations. Directions for future work include analytically establishing error bounds on the trajectories returned by reduced-order models in the face of parametric variations in the filter and control parameters.

Appendix

A. Steady-state Operation of PLL

Express the grid voltage as $v_g = V_g \sin(\delta_g)$, where V_g and δ_g are the voltage amplitude and angle, respectively. The corresponding $\alpha\beta$ components of v_g are given by

$$v_g^\alpha = v_g = V_g \sin(\delta_g),$$
$$v_g^\beta = V_g \sin\left(\delta_g - \frac{\pi}{2}\right) = -V_g \cos(\delta_g).$$

The d-axis component of v_g is obtained from (2) as

$$v_g^d = V_g \cos(\delta)\sin(\delta_g) - V_g \sin(\delta)\cos(\delta_g) = V_g \sin(\delta_g - \delta).$$

From above, it follows that when $\delta = \delta_g$, $v_g^d = 0$.

This article has been accepted for publication in a future issue of this journal, but has not been fully edited. Content may change prior to final publication. Citation information: DOI 10.1109/TEC.2018.2881710, IEEE Transactions on Energy Conversion

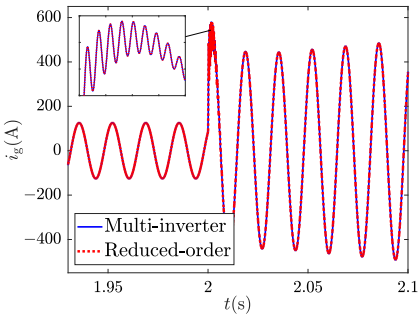

(a) Case #1

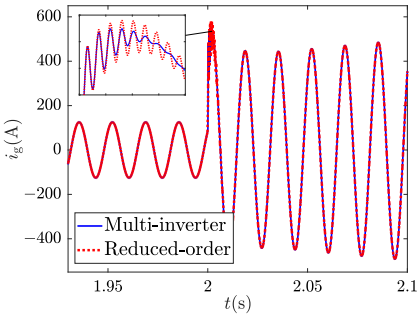

(b) Case #2

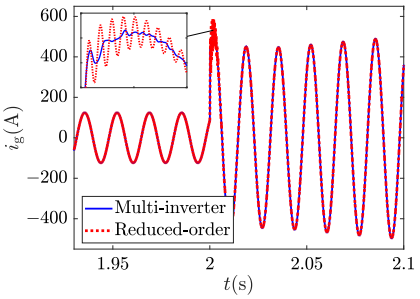

(c) Case #3

Figure 6: Simulation results comparing the injected current for a system of 100 parallel-connected inverters with all inverter dynamics simulated superimposed to results from the reduced-order model for the following cases: (a) heterogeneous power ratings with power-scaling parameters (κ) vary between 0.5 and 5, (b) identical power ratings with $\kappa = 1$ and LCL-filter parameters vary between $\pm 10\%$ of their nominal values,(c) same setup as (b), but with variation of $\pm 80\%$.

B. State-space Model Particulars

$$A_{LCL} = \begin{bmatrix} -\frac{R_i}{L_i} & 0 & 0 & 0 \\ \omega_{nom} + \frac{R_i}{L_i} & -\omega_{nom} & 0 & 0 \\ 0 & 0 & -\frac{R_g}{L_g} & 0 \\ 0 & 0 & \omega_{nom} + \frac{R_g}{L_g} & -\omega_{nom} \\ -R_f\frac{R_i}{L_i} + \frac{1}{C_f} & 0 & R_f\frac{R_g}{L_g} - \frac{1}{C_f} & 0 \\ R_f\frac{R_i}{L_i} - \frac{1}{C_f} & 0 & -R_f\frac{R_g}{L_g} + \frac{1}{C_f} & 0 \end{bmatrix}$$

$$\begin{bmatrix} 0 & 0 \\ 0 & 0 \\ \frac{1}{L_g} & 0 \\ -\frac{1}{L_g} & 0 \\ -\frac{R_f}{L_g} & 0 \\ \omega_{nom} + \frac{R_f}{L_g} & -\omega_{nom} \end{bmatrix}, A_{CC} = \begin{bmatrix} 0 & -k^p_{PC} \\ -k^p_{PC} & 0 \\ 0 & k^i_{PC} \\ k^i_{PC} & 0 \end{bmatrix}^T,$$

$$A_{PC} = \begin{bmatrix} -\omega_{c,PC} & 0 & 0 & 0 \\ 0 & -\omega_{c,PC} & 0 & 0 \\ -1 & 0 & 0 & 0 \\ 0 & -1 & 0 & 0 \end{bmatrix}, B_{CC} = \begin{bmatrix} 0 & k^p_{PC} \\ k^p_{PC} & 0 \end{bmatrix},$$

$$A_{PLL} = \begin{bmatrix} -\omega_{nom} & 0 & 0 & 0 \\ 0 & -\omega_{c,PLL} & 0 & 0 \\ 0 & -1 & 0 & 0 \\ 0 & -k^p_{PLL} & k^i_{PLL} & 0 \end{bmatrix}, B_{PLL} = \begin{bmatrix} 0 & -1 \\ 0 & 0 \\ 0 & 0 \\ 0 & 0 \end{bmatrix},$$

$$B_{LCL} = \begin{bmatrix} 0 & 0 & 0 & 0 & 0 & 0 \\ 0 & 0 & -\frac{1}{L_g} & \frac{1}{L_g} & \frac{R_f}{L_g} & -\frac{R_f}{L_g} \end{bmatrix}^T, B_{PC} = \begin{bmatrix} 0 & 0 \\ 0 & 0 \\ 1 & 0 \\ 0 & 1 \end{bmatrix}.$$

Lastly, the entries of $g(x, u_1, u_2)$, with g_ℓ denotes the ℓ-th entry of $g(x, u_1, u_2)$, are

$$\begin{aligned} g_1 &= \frac{1}{L_i}\left(k^p_{CC}(i^{d*}_i - i^\alpha_i \cos\delta - i^\beta_i \sin\delta) + k^i_{CC}\gamma^d\right)\cos\delta \\ &\quad - \frac{1}{L_i}\left(k^p_{CC}(i^{q*}_i + i^\alpha_i \sin\delta - i^\beta_i \cos\delta) + k^i_{CC}\gamma^q\right)\sin\delta, \\ g_2 &= \eta(i^\alpha_i - i^\beta_i) - g_1, \quad g_3 = 0, \quad g_4 = 0, \\ g_5 &= R_f g_1, \quad g_6 = \eta(v^\alpha_f - v^\beta_f) - g_5, \\ g_7 &= -i^\alpha_i \cos\delta - i^\beta_i \sin\delta, \quad g_8 = i^\alpha_i \sin\delta - i^\beta_i \cos\delta, \\ g_9 &= \frac{\omega_{c,PC}}{2}(v_g i^\alpha_g + v^\beta_g i^\beta_g), \quad g_{10} = \frac{\omega_{c,PC}}{2}(v^\beta_g i^\alpha_g - v_g i^\beta_g), \\ g_{11} &= 0, \quad g_{12} = 0, \quad g_{13} = \eta(v_g - v^\beta_g), \\ g_{14} &= \omega_{c,PLL}(v_g \cos\delta + v^\beta_g \sin\delta), \quad g_{15} = 0, \quad g_{16} = \omega_{nom}, \end{aligned}$$

where $\eta := -k^p_{PLL} v_{PLL} + k^i_{PLL}\phi_{PLL}$, $i^{d*}_i = k^p_{PC}(q^* - q_{avg}) + k^i_{PC}\phi^q$, and $i^{q*}_i = k^p_{PC}(p^* - p_{avg}) + k^i_{PC}\phi^p$.

C. Proof of Corollary 1

We begin by noting that the PLL dynamics are decoupled, and the its parameters in the individual and reduced-order models are the same, therefore $\forall t \geq t_0$, $x^r_{PLL}(t) = x_{PLL,\ell}(t)\ \forall \ell$ if we initialize $x^r_{PLL}(t_0) = x_{PLL,\ell}(t_0)\ \forall \ell$. Next, partition the permuted versions of (12) and (16), excluding the PLL dynamics, as

$$\begin{aligned} \begin{bmatrix} \dot\lambda_\ell \\ \dot v^{\alpha\beta}_{f,\ell} \end{bmatrix} &= \begin{bmatrix} \widehat A_{11} & \widehat A_{12} \\ \widehat A_{21} & \widehat A_{22} \end{bmatrix}\begin{bmatrix} \lambda_\ell \\ v^{\alpha\beta}_{f,\ell} \end{bmatrix} + \begin{bmatrix} \widehat B_{11} \\ \widehat B_{12} \end{bmatrix} u_{1,\ell} + \begin{bmatrix} \widehat B_{21} \\ \widehat B_{22} \end{bmatrix} u_2 \\ &\quad + \begin{bmatrix} \widehat g_1(\widehat x_\ell, u_{1,\ell}, u_2) \\ \widehat g_2(\widehat x_\ell, u_{1,\ell}, u_2) \end{bmatrix}, \end{aligned} \tag{45}$$

$$\begin{aligned} \begin{bmatrix} \dot\lambda^r \\ \dot v^{\alpha\beta,r}_f \end{bmatrix} &= \begin{bmatrix} \widehat A^r_{11} & \widehat A^r_{12} \\ \widehat A^r_{21} & \widehat A^r_{22} \end{bmatrix}\begin{bmatrix} \lambda^r \\ v^{\alpha\beta,r}_f \end{bmatrix} + \begin{bmatrix} \widehat B^r_{11} \\ \widehat B^r_{12} \end{bmatrix} u^r_1 + \begin{bmatrix} \widehat B^r_{21} \\ \widehat B^r_{22} \end{bmatrix} u^r_2 \\ &\quad + \begin{bmatrix} \widehat g^r_1(\widehat x^r, u^r_1, u^r_2) \\ \widehat g^r_2(\widehat x^r, u^r_1, u^r_2) \end{bmatrix}, \end{aligned} \tag{46}$$

This article has been accepted for publication in a future issue of this journal, but has not been fully edited. Content may change prior to final publication. Citation information: DOI 10.1109/TEC.2018.2881710, IEEE Transactions on Energy Conversion

where $\widehat{g}_1 : \mathbb{R}^{16}\times\mathbb{R}^2\times\mathbb{R}^2 \to \mathbb{R}^{10}$ and $\widehat{g}_2 : \mathbb{R}^{16}\times\mathbb{R}^2\times\mathbb{R}^2 \to \mathbb{R}^2$ are the nonlinear parts of the dynamics of λ_ℓ and $v_{\mathrm{f},\ell}^{\alpha\beta}$, respectively (similarly for $\widehat{g}_1^{\mathrm{r}}$ and $\widehat{g}_2^{\mathrm{r}}$). We bring to note a slight abuse of notation in terms of the submatrices in (45) and (46) and those in (22) and (23). Furthermore, the submatrices in (45) and (46) also follow the relationships in (24). Define $z_1 := \lambda^{\mathrm{r}} - \sum_{\ell=1}^{N}\lambda_\ell$ and $z_2 := Nv_{\mathrm{f}}^{\alpha\beta,\mathrm{r}} - \sum_{\ell=1}^{N} v_{\mathrm{f},\ell}^{\alpha\beta}$. The dynamics of z_1 and z_2 are:

$$\dot{z}_1 = \dot{\lambda}^{\mathrm{r}} - \sum_{\ell=1}^{N}\dot{\lambda}_\ell = \widehat{A}_{11}^{\mathrm{r}}\lambda^{\mathrm{r}} + \widehat{A}_{12}^{\mathrm{r}}v_{\mathrm{f}}^{\alpha\beta,\mathrm{r}} + \widehat{B}_{11}^{\mathrm{r}}u_1^{\mathrm{r}} + \widehat{B}_{21}^{\mathrm{r}}u_2^{\mathrm{r}} + \widehat{g}_1^{\mathrm{r}}(\widehat{x}^{\mathrm{r}}, u_1^{\mathrm{r}}, u_2^{\mathrm{r}}) - \sum_{\ell=1}^{N}\Big(\widehat{A}_{11}\lambda_\ell + \widehat{A}_{12}v_{\mathrm{f},\ell}^{\alpha\beta,\mathrm{r}} + \widehat{B}_{11}u_{1,\ell} + \widehat{B}_{21}u_2 + \widehat{g}_1(\widehat{x}_\ell, u_{1,\ell}, u_2^{\mathrm{r}})\Big), \tag{47}$$

$$\dot{z}_2 = N\dot{v}_{\mathrm{f}}^{\alpha\beta,\mathrm{r}} - \sum_{\ell=1}^{N}\dot{v}_{\mathrm{f},\ell}^{\alpha\beta} = N\Big(\widehat{A}_{21}^{\mathrm{r}}\lambda^{\mathrm{r}} + \widehat{A}_{21}^{\mathrm{r}}v_{\mathrm{f}}^{\alpha\beta,\mathrm{r}} + \widehat{B}_{12}^{\mathrm{r}}u_1^{\mathrm{r}} + \widehat{B}_{22}^{\mathrm{r}}u_2^{\mathrm{r}} + \widehat{g}_2^{\mathrm{r}}(\widehat{x}^{\mathrm{r}}, u_1^{\mathrm{r}}, u_2^{\mathrm{r}})\Big) - \sum_{\ell=1}^{N}\Big(\widehat{A}_{21}\lambda_\ell + \widehat{A}_{22}v_{\mathrm{f},\ell}^{\alpha\beta,\mathrm{r}} + \widehat{B}_{12}u_{1,\ell} + \widehat{B}_{22}u_2 + \widehat{g}_2(\widehat{x}_\ell, u_{1,\ell}, u_2^{\mathrm{r}})\Big). \tag{48}$$

Next, we will show that

$$\widehat{g}_1^{\mathrm{r}}(\widehat{x}^{\mathrm{r}}, u_1^{\mathrm{r}}, u_2^{\mathrm{r}}) - \sum_{\ell=1}^{N}\widehat{g}_1(\widehat{x}_\ell, u_{1,\ell}, u_2) = \widehat{g}_1(\chi, 0_2, u_2), \tag{49}$$

$$N\widehat{g}_2^{\mathrm{r}}(\widehat{x}^{\mathrm{r}}, u_1^{\mathrm{r}}, u_2^{\mathrm{r}}) - \sum_{\ell=1}^{N}\widehat{g}_2(\widehat{x}_\ell, u_{1,\ell}, u_2) = \widehat{g}_2(\chi, 0_2, u_2), \tag{50}$$

where $\chi := [z_1^{\mathrm{T}}, z_2^{\mathrm{T}}, x_{\mathrm{PLL}}^{\mathrm{rT}}]^{\mathrm{T}}$. Let $\widehat{g}_{1,k}(\widehat{x}_\ell)$, $\widehat{g}_{2,k}(\widehat{x}_\ell)$, $\widehat{g}_{1,k}^{\mathrm{r}}(\widehat{x}^{\mathrm{r}})$, and $\widehat{g}_{2,k}^{\mathrm{r}}(\widehat{x}^{\mathrm{r}})$ denote the k-th entries of $\widehat{g}_1(\widehat{x}_\ell, u_{1,\ell}, u_2)$, $\widehat{g}_2(\widehat{x}_\ell, u_{1,\ell}, u_2)$, $\widehat{g}_1^{\mathrm{r}}(\widehat{x}^{\mathrm{r}}, u_1^{\mathrm{r}}, u_2^{\mathrm{r}})$, and $\widehat{g}_2^{\mathrm{r}}(\widehat{x}^{\mathrm{r}}, u_1^{\mathrm{r}}, u_2^{\mathrm{r}})$, respectively. Then, we have

$$\widehat{g}_{1,1}^{\mathrm{r}}(\widehat{x}^{\mathrm{r}}) - \sum_{\ell=1}^{N}\widehat{g}_{1,1}(\widehat{x}_\ell) = \frac{N}{L_{\mathrm{i}}}\Bigg[\Bigg(\frac{k_{\mathrm{CC}}^p}{N}\Bigg(k_{\mathrm{PC}}^p(\sum_{\ell=1}^{N}q_\ell^* - q_{\mathrm{avg}}^{\mathrm{r}}) + k_{\mathrm{PC}}^i\phi^{\mathrm{q,r}} - i_{\mathrm{i}}^{\mathrm{d,r}}\Bigg) + \frac{k_{\mathrm{CC}}^i}{N}\gamma^{\mathrm{d,r}}\Bigg)\cos\delta^{\mathrm{r}} - \Bigg(\frac{k_{\mathrm{CC}}^p}{N}\Bigg(k_{\mathrm{PC}}^p(\sum_{\ell=1}^{N}p_\ell^* - p_{\mathrm{avg}}^{\mathrm{r}}) + k_{\mathrm{PC}}^i\phi^{\mathrm{p}} - i_{\mathrm{i}}^{\mathrm{q,r}}\Bigg) - \frac{k_{\mathrm{CC}}^i}{N}\gamma^{\mathrm{q,r}}\Bigg)\sin\delta^{r}\Bigg] - \sum_{\ell=1}^{N}\Bigg(\Bigg(\frac{k_{\mathrm{CC}}^p}{L_{\mathrm{i}}}\Big(k_{\mathrm{PC}}^p(q_\ell^* - q_{\mathrm{avg},\ell}) + k_{\mathrm{PC}}^i\phi_\ell^{\mathrm{q}} - i_{\mathrm{i},\ell}^{\mathrm{d}}\Big) + \frac{k_{\mathrm{CC}}^i}{L_{\mathrm{i}}}\gamma_\ell^{\mathrm{d}}\Bigg)\cos\delta_\ell + \frac{k_{\mathrm{CC}}^p}{L_{\mathrm{i}}}\Bigg(\Big(k_{\mathrm{PC}}^p(p_\ell^* - p_{\mathrm{avg},\ell}) + k_{\mathrm{PC}}^i\phi^{\mathrm{p}} - i_{\mathrm{i}}^{\mathrm{q,r}}\Big) - \frac{k_{\mathrm{CC}}^i}{N}\gamma^{\mathrm{q,r}}\Bigg)\sin\delta_\ell\Bigg)$$
$$= \Bigg(\frac{k_{\mathrm{CC}}^p}{L_{\mathrm{i}}}\Bigg(k_{\mathrm{PC}}^p(0 - (q_{\mathrm{avg}}^{\mathrm{r}} - \sum_{\ell=1}^{N}q_{\mathrm{avg},\ell})) + k_{\mathrm{PC}}^i(\phi^{\mathrm{q},r} - \sum_{\ell=1}^{N}\phi_\ell^{\mathrm{q}}) - (i_{\mathrm{i}}^{\mathrm{d,r}} - \sum_{\ell=1}^{N}i_{\mathrm{i},\ell}^{\mathrm{d}})\Bigg) + \frac{k_{\mathrm{CC}}^i}{L_{\mathrm{i}}}(\gamma^{\mathrm{d,r}} - \sum_{\ell=1}^{N}\gamma_\ell^{\mathrm{d}})\Bigg)\cos\delta^{\mathrm{r}} + \Bigg(\frac{k_{\mathrm{CC}}^p}{L_{\mathrm{i}}}\Bigg(k_{\mathrm{PC}}^p(0 - (p_{\mathrm{avg}}^{\mathrm{r}} - \sum_{\ell=1}^{N}p_{\mathrm{avg},\ell})) + k_{\mathrm{PC}}^i(\phi^{\mathrm{p},r} - \sum_{\ell=1}^{N}\phi_\ell^{\mathrm{p}}) - (i_{\mathrm{i}}^{\mathrm{q,r}} - \sum_{\ell=1}^{N}i_{\mathrm{i},\ell}^{\mathrm{q}})\Bigg) + \frac{k_{\mathrm{CC}}^i}{L_{\mathrm{i}}}(\gamma^{\mathrm{q,r}} - \sum_{\ell=1}^{N}\gamma_\ell^{\mathrm{q}})\Bigg)\sin\delta^{\mathrm{r}}$$
$$= \widehat{g}_{1,1}(\chi, 0_2, u_2), \tag{51}$$

$$\widehat{g}_{1,2}^{\mathrm{r}}(\widehat{x}^{\mathrm{r}}) - \sum_{\ell=1}^{N}\widehat{g}_{1,2}(\widehat{x}_\ell) = (-k_{\mathrm{PLL}}^p v_{\mathrm{PLL}}^{\mathrm{r}} + k_{\mathrm{PLL}}^i\phi_{\mathrm{PLL}}^{\mathrm{r}})(i_{\mathrm{i}}^{\alpha,\mathrm{r}} - i_{\mathrm{i}}^{\beta,\mathrm{r}}) - \widehat{g}_{1,1}^{\mathrm{r}}(\widehat{x}^{\mathrm{r}}) - \sum_{\ell=1}^{N}\Big((-k_{\mathrm{PLL}}^p v_{\mathrm{PLL},\ell} + k_{\mathrm{PLL}}^i\phi_{\mathrm{PLL},\ell})(i_{\mathrm{i},\ell}^{\alpha} - i_{\mathrm{i},\ell}^{\beta}) - \widehat{g}_{1,1}(\widehat{x}_\ell)\Big) = (-k_{\mathrm{PLL}}^p v_{\mathrm{PLL}}^{\mathrm{r}} + k_{\mathrm{PLL}}^i\phi_{\mathrm{PLL}}^{\mathrm{r}})\Big((i_{\mathrm{i}}^{\alpha,\mathrm{r}} - \sum_{\ell=1}^{N}i_{\mathrm{i},\ell}^{\alpha}) + (i_{\mathrm{i}}^{\beta,\mathrm{r}} - \sum_{\ell=1}^{N}i_{\mathrm{i},\ell}^{\beta})\Big) - \Big(\widehat{g}_{1,1}^{\mathrm{r}}(\widehat{x}^{\mathrm{r}}) - \sum_{\ell=1}^{N}\widehat{g}_{1,1}(\widehat{x}_\ell)\Big)$$
$$= \widehat{g}_{1,2}(\chi, 0_2, u_2), \tag{52}$$

$$\widehat{g}_{1,3}^{\mathrm{r}}(\widehat{x}^{\mathrm{r}}) - \sum_{\ell=1}^{N}\widehat{g}_{1,3}(\widehat{x}_\ell) = 0 = \widehat{g}_{1,3}(\chi, 0_2, u_2), \tag{53}$$

$$\widehat{g}_{1,4}^{\mathrm{r}}(\widehat{x}^{\mathrm{r}}) - \sum_{\ell=1}^{N}\widehat{g}_{1,4}(\widehat{x}_\ell) = 0 = \widehat{g}_{1,4}(\chi, 0_2, u_2), \tag{54}$$

$$\widehat{g}_{1,5}^{\mathrm{r}}(\widehat{x}^{\mathrm{r}}) - \sum_{\ell=1}^{N}\widehat{g}_{1,5}(\widehat{x}_\ell) = -i_{\mathrm{i}}^{\alpha,\mathrm{r}}\cos\delta^{\mathrm{r}} - i_{\mathrm{i}}^{\beta,\mathrm{r}}\sin\delta^{\mathrm{r}} - \sum_{\ell=1}^{N}\Big(-i_{\mathrm{i},\ell}^{\alpha}\cos\delta_\ell - i_{\mathrm{i},\ell}^{\beta}\sin\delta_\ell\Big) = -(i_{\mathrm{i}}^{\alpha,\mathrm{r}} - \sum_{\ell=1}^{N}i_{\mathrm{i},\ell}^{\alpha})\cos\delta^{\mathrm{r}} - (i_{\mathrm{i}}^{\beta,\mathrm{r}} - \sum_{\ell=1}^{N}i_{\mathrm{i},\ell}^{\beta})\sin\delta^{\mathrm{r}} = \widehat{g}_{1,5}(\chi, 0_2, u_2), \tag{55}$$

$$\widehat{g}_{1,6}^{\mathrm{r}}(\widehat{x}^{\mathrm{r}}) - \sum_{\ell=1}^{N}\widehat{g}_{1,6}(\widehat{x}_\ell) = i_{\mathrm{i}}^{\alpha,\mathrm{r}}\sin\delta^{\mathrm{r}} - i_{\mathrm{i}}^{\beta,\mathrm{r}}\cos\delta^{\mathrm{r}} - \sum_{\ell=1}^{N}\Big(i_{\mathrm{i},\ell}^{\alpha}\sin\delta_\ell - i_{\mathrm{i},\ell}^{\beta}\cos\delta_\ell\Big) = (i_{\mathrm{i}}^{\alpha,\mathrm{r}} - \sum_{\ell=1}^{N}i_{\mathrm{i},\ell}^{\alpha})\sin\delta^{\mathrm{r}} - (i_{\mathrm{i}}^{\beta,\mathrm{r}} - \sum_{\ell=1}^{N}i_{\mathrm{i},\ell}^{\beta})\cos\delta^{\mathrm{r}} = \widehat{g}_{1,6}(\chi, 0_2, u_2), \tag{56}$$

$$\widehat{g}_{1,7}^{\mathrm{r}}(\widehat{x}^{\mathrm{r}}) - \sum_{\ell=1}^{N}\widehat{g}_{1,7}(\widehat{x}_\ell) = \frac{\omega_{\mathrm{c,PC}}}{2}(v_{\mathrm{g}}i_{\mathrm{g}}^{\alpha,\mathrm{r}} + v_{\mathrm{g}}^{\beta,\mathrm{r}}i_{\mathrm{g}}^{\beta,\mathrm{r}}) - \sum_{\ell=1}^{N}\frac{\omega_{\mathrm{c,PC}}}{2}\Big(v_{\mathrm{g}}i_{\mathrm{g},\ell}^{\alpha} + v_{\mathrm{g},\ell}^{\beta}i_{\mathrm{g},\ell}^{\beta}\Big) = \frac{\omega_{\mathrm{c,PC}}}{2}\Big(v_{\mathrm{g}}(i_{\mathrm{g}}^{\alpha,\mathrm{r}} - \sum_{\ell=1}^{N}i_{\mathrm{g},\ell}^{\alpha}) + v_{\mathrm{g}}^{\beta,\mathrm{r}}(i_{\mathrm{g}}^{\beta,\mathrm{r}} - \sum_{\ell=1}^{N}i_{\mathrm{g},\ell}^{\beta})\Big) = \widehat{g}_{1,7}(\chi, 0_2, u_2), \tag{57}$$

$$\widehat{g}_{1,8}^{\mathrm{r}}(\widehat{x}^{\mathrm{r}}) - \sum_{\ell=1}^{N}\widehat{g}_{1,8}(\widehat{x}_\ell) = \frac{\omega_{\mathrm{c,PC}}}{2}(v_{\mathrm{g}}^{\beta,\mathrm{r}}i_{\mathrm{g}}^{\alpha,\mathrm{r}} - v_{\mathrm{g}}i_{\mathrm{g}}^{\beta,\mathrm{r}}) - \sum_{\ell=1}^{N}\frac{\omega_{\mathrm{c,PC}}}{2}\Big(v_{\mathrm{g},\ell}^{\beta}i_{\mathrm{g},\ell}^{\alpha} - v_{\mathrm{g}}i_{\mathrm{g},\ell}^{\beta}\Big) = \frac{\omega_{\mathrm{c,PC}}}{2}\Big(v_{\mathrm{g}}^{\beta,\mathrm{r}}(i_{\mathrm{g}}^{\alpha,\mathrm{r}} - \sum_{\ell=1}^{N}i_{\mathrm{g},\ell}^{\alpha}) - v_{\mathrm{g}}(i_{\mathrm{g}}^{\beta,\mathrm{r}} - \sum_{\ell=1}^{N}i_{\mathrm{g},\ell}^{\beta})\Big) = \widehat{g}_{1,8}(\chi, 0_2, u_2), \tag{58}$$

$$\widehat{g}_{1,9}^{\mathrm{r}}(\widehat{x}^{\mathrm{r}}) - \sum_{\ell=1}^{N}\widehat{g}_{1,9}(\widehat{x}_\ell) = 0 = \widehat{g}_{1,9}(\chi, 0_2, u_2), \tag{59}$$

This article has been accepted for publication in a future issue of this journal, but has not been fully edited. Content may change prior to final publication. Citation information: DOI 10.1109/TEC.2018.2881710, IEEE Transactions on Energy Conversion

$$\widehat{g}^{\mathrm{r}}_{1,10}(\widehat{x}^{\mathrm{r}}) - \sum_{\ell=1}^{N} \widehat{g}_{1,10}(\widehat{x}_\ell) = 0 = \widehat{g}_{1,10}(\chi, 0_2, u_2), \tag{60}$$

$$N\widehat{g}^{\mathrm{r}}_{2,1}(\widehat{x}^{\mathrm{r}}) - \sum_{\ell=1}^{N} \widehat{g}_{2,1}(\widehat{x}_\ell) = N\frac{R_{\mathrm{f}}}{N}\widehat{g}^{\mathrm{r}}_{1,1}(\widehat{x}^{\mathrm{r}}) - R_{\mathrm{f}}\sum_{\ell=1}^{N} \widehat{g}_{1,1}(\widehat{x}_\ell)$$

$$= R_{\mathrm{f}}(\widehat{g}^{\mathrm{r}}_{1,1}(\widehat{x}^{\mathrm{r}}) - \sum_{\ell=1}^{N} \widehat{g}_{1,1}(\widehat{x}_\ell)) = \widehat{g}_{2,1}(\chi, 0_2, u_2), \tag{61}$$

$$N\widehat{g}^{\mathrm{r}}_{2,2}(\widehat{x}^{\mathrm{r}}) - \sum_{\ell=1}^{N} \widehat{g}_{2,2}(\widehat{x}_\ell) = N(-k^p_{\mathrm{PLL}} v^{\mathrm{r}}_{\mathrm{PLL}} + k^i_{\mathrm{PLL}}\phi^{\mathrm{r}}_{\mathrm{PLL}})$$

$$(v^{\alpha,\mathrm{r}}_{\mathrm{f}} - v^{\beta,\mathrm{r}}_{\mathrm{f}}) - N\widehat{g}^{\mathrm{r}}_{2,1}(\widehat{x}^{\mathrm{r}}) - \sum_{\ell=1}^{N} \Big((-k^p_{\mathrm{PLL}} v_{\mathrm{PLL},\ell}$$

$$+ k^i_{\mathrm{PLL}}\phi_{\mathrm{PLL},\ell})(v^{\alpha}_{\mathrm{f},\ell} - v^{\beta}_{\mathrm{f},\ell}) - \widehat{g}_{2,1}(\widehat{x}_\ell)\Big) = (-k^p_{\mathrm{PLL}} v^{\mathrm{r}}_{\mathrm{PLL}}$$

$$+ k^i_{\mathrm{PLL}}\phi^{\mathrm{r}}_{\mathrm{PLL}})\Big((Nv^{\alpha,\mathrm{r}}_{\mathrm{f}} - \sum_{\ell=1}^{N} v^{\alpha}_{\mathrm{f},\ell}) - (Nv^{\beta,\mathrm{r}}_{\mathrm{f}} - \sum_{\ell=1}^{N} v^{\beta}_{\mathrm{f},\ell})\Big)$$

$$- (N\widehat{g}^{\mathrm{r}}_{2,1}(\widehat{x}^{\mathrm{r}}) - \sum_{\ell=1}^{N} \widehat{g}_{2,1}(\widehat{x}_\ell)) = \widehat{g}_{2,2}(\chi, 0_2, u_2). \tag{62}$$

Therefore, (49) and (50) hold. Using identities (24), (49) and (50), we can write the dynamics of z_1 and z_2 as

$$\dot{z}_1 = A_{11}z_1 + A_{12}z_2 + \widehat{g}_1(\chi, 0_2, u_2), \tag{63}$$

$$\dot{z}_2 = A_{21}z_1 + A_{22}z_2 + \widehat{g}_2(\chi, 0_2, u_2). \tag{64}$$

If we initialize $z_1(t_0) = 0_{10}$ and $z_2(t_0) = 0_2$, we have $z_1(t) = 0_{10}, z_2(t) = 0_2, \forall t \geq t_0$ since $g_1(\chi, 0_2, u_2) = 0_{10}$ and $g_2(\chi, 0_2, u_2) = 0_2$ when $z_1 = 0_{10}$ and $z_2 = 0_2$. By the definition of z_1 and z_2, we have $\lambda^{\mathrm{r}}(t) = \sum_{\ell=1}^{N} \lambda_\ell(t), v^{\alpha\beta,\mathrm{r}}_{\mathrm{f}}(t) = \frac{1}{N}\sum_{\ell=1}^{N} v^{\alpha\beta}_{\mathrm{f},\ell}(t), \forall t \geq t_0$.

For the other direction, given that $\forall t \geq t_0$: $z_1(t) = \lambda^{\mathrm{T}}(t) - \sum_{\ell=1}^{N} \lambda_\ell(t) = 0_{10}, z_2(t) = Nv^{\alpha\beta,\mathrm{r}}_{\mathrm{f}}(t) - \sum_{\ell=1}^{N} v^{\alpha\beta}_{\mathrm{f},\ell}(t) = 0_2, x^{\mathrm{r}}_{\mathrm{PLL}}(t) = x_{\mathrm{PLL},\ell}(t), \forall \ell$, (47) and (48) can be written as

$$0_{10} = (\widehat{A}^{\mathrm{r}}_{11} - \widehat{A}_{11})\lambda^{\mathrm{r}} + (\widehat{A}^{\mathrm{r}}_{12} - N\widehat{A}_{12})v^{\alpha\beta,\mathrm{r}}_{\mathrm{f}} + (\widehat{B}^{\mathrm{r}}_{11} - \widehat{B}_{11})u^{\mathrm{r}}_1$$
$$+ (\widehat{B}^{\mathrm{r}}_{21} - N\widehat{B}_{21})u^{\mathrm{r}}_2 + \widehat{g}^{\mathrm{r}}_1(\widehat{x}^{\mathrm{r}}, u^{\mathrm{r}}_1, u^{\mathrm{r}}_2) - \sum_{\ell=1}^{N} \widehat{g}_1(\widehat{x}_\ell, u_{1,\ell}, u^{\mathrm{r}}_2),$$

$$0_2 = (N\widehat{A}^{\mathrm{r}}_{21} - \widehat{A}_{21})\lambda^{\mathrm{r}} + (N\widehat{A}^{\mathrm{r}}_{22} - N\widehat{A}_{22})v^{\alpha\beta,\mathrm{r}}_{\mathrm{f}} + (N\widehat{B}^{\mathrm{r}}_{21}$$
$$- \widehat{B}_{21})u^{\mathrm{r}}_1 + (N\widehat{B}^{\mathrm{r}}_{22} - N\widehat{B}_{22})u^{\mathrm{r}}_2 + N\widehat{g}^{\mathrm{r}}_2(\widehat{x}^{\mathrm{r}}, u^{\mathrm{r}}_1, u^{\mathrm{r}}_2)$$
$$- \sum_{\ell=1}^{N} \widehat{g}_2(\widehat{x}_\ell, u_{1,\ell}, u^{\mathrm{r}}_2).$$

These equalities are satisfied when the following identities hold:

$$\begin{aligned} &\widehat{A}^{\mathrm{r}}_{11} = \widehat{A}_{11},\ \widehat{A}^{\mathrm{r}}_{12} = N\widehat{A}_{12},\ \widehat{A}^{\mathrm{r}}_{21} = \frac{1}{N}\widehat{A}_{21},\ \widehat{A}^{\mathrm{r}}_{22} = \widehat{A}_{22}, \\ &\widehat{B}^{\mathrm{r}}_{11} = \widehat{B}_{11},\ \widehat{B}^{\mathrm{r}}_{21} = N\widehat{B}_{21},\ \widehat{B}^{\mathrm{r}}_{12} = \frac{1}{N}\widehat{B}_{12},\ \widehat{B}^{\mathrm{r}}_{22} = \widehat{B}_{22}, \end{aligned} \tag{65}$$

$$\widehat{g}^{\mathrm{r}}_1(\widehat{x}^{\mathrm{r}}, u^{\mathrm{r}}_1, u^{\mathrm{r}}_2) = \sum_{\ell=1}^{N} \widehat{g}_1(\widehat{x}_\ell, u_{1,\ell}, u_2), \tag{66}$$

$$N\widehat{g}^{\mathrm{r}}_2(\widehat{x}^{\mathrm{r}}, u^{\mathrm{r}}_1, u^{\mathrm{r}}_2) = \sum_{\ell=1}^{N} \widehat{g}_2(\widehat{x}_\ell, u_{1,\ell}, u_2). \tag{67}$$

It is straightforward to see that (17a) and the unscaled parameters are the only set of parameters that satisfy (65). For the rest of parameters, i.e., R_{i}, L_{i}, k^p_{CC}, and k^i_{CC}, it can be derived that they always appear in (65)–(67) as fractions of $\frac{R_{\mathrm{i}}}{L_{\mathrm{i}}}$, $\frac{k^p_{\mathrm{CC}}}{L_{\mathrm{i}}}$, and $\frac{k^i_{\mathrm{CC}}}{L_{\mathrm{i}}}$. Therefore, they are related to those in the reduced-order model through (17b). This concludes the proof.

REFERENCES

[1] J. A. Taylor, S. V. Dhople, and D. S. Callaway, "Power systems without fuel," *Renewable and Sustainable Energy Reviews*, vol. 57, pp. 1322–1336, 2016.

[2] "800,000 Microinverters Remotely Retrofitted on Oahu in One Day." http://spectrum.ieee.org/energywise/green-tech/solar/in-one-day-800000-microinverters-remotely-retrofitted-on-oahu. Accessed: 2017-03-14.

[3] "Our Plans for the Future." https://www.hawaiianelectric.com/clean-energy-hawaii. Accessed: 2018-01-23.

[4] "REthinking Energy 2017: Accelerating the global energy transformation." http://www.irena.org/DocumentDownloads/Publications/IRENA_REthinking_Energy_2017.pdf. Accessed: 2017-10-27.

[5] J. H. Chow, *Power System Coherency and Model Reduction*. Springer, 2013.

[6] S. D. Pekarek, M. T. Lemanski, and E. A. Walters, "On the use of singular perturbations to neglect the dynamic saliency of synchronous machines," *IEEE Transactions on Energy Conversion*, vol. 17, pp. 385–391, September 2002.

[7] H. You, V. Vittal, and X. Wang, "Slow coherency-based islanding," *IEEE Transactions on Power Systems*, vol. 19, pp. 483–491, February 2004.

[8] M. L. Ourari, L. A. Dessaint, and V.-Q. Do, "Dynamic equivalent modeling of large power systems using structure preservation technique," *IEEE Transactions on Power Systems*, vol. 21, pp. 1284–1295, August 2006.

[9] A. J. Germond and R. Podmore, "Dynamic aggregation of generating unit models," *IEEE Transactions on Power Apparatus and Systems*, vol. PAS-97, pp. 1060–1069, July 1978.

[10] E. Muljadi, S. Pasupulati, A. Ellis, and D. Kosterov, "Method of equivalencing for a large wind power plant with multiple turbine representation," in *2008 IEEE Power and Energy Society General Meeting - Conversion and Delivery of Electrical Energy in the 21st Century*, pp. 1–9, July 2008.

[11] S. Izadkhast, P. Garcia-Gonzalez, P. Frias, L. Ramirez-Elizondo, and P. Bauer, "An aggregate model of plug-in electric vehicles including distribution network characteristics for primary frequency control," *IEEE Transactions on Power Systems*, vol. 31, pp. 2987–2998, July 2016.

[12] J. Zhang and A. Domínguez-García, "Evaluation of demand response resource aggregation system capacity under uncertainty," *IEEE Transactions on Smart Grid*, vol. PP, no. 99, pp. 1–1, 2017.

[13] M. Rasheduzzaman, J. A. Mueller, and J. W. Kimball, "Reduced-order small-signal model of microgrid systems," *IEEE Transactions on Sustainable Energy*, vol. 6, pp. 1292–1305, October 2015.

[14] L. Luo and S. V. Dhople, "Spatiotemporal model reduction of inverter-based islanded microgrids," *IEEE Transactions on Energy Conversion*, vol. 29, pp. 823–832, December 2014.

[15] K. Kodra, N. Zhong, and Z. Gajić, "Model order reduction of an islanded microgrid using singular perturbations," in *American Control Conference (ACC)*, pp. 3650–3655, July 2016.

[16] O. O. Ajala, A. D. Domínguez-García, and P. W. Sauer, "A hierarchy of models for inverter-based microgrids," in *Energy Markets and Responsive Grids: Modeling, Control and Optimization* (S. Meyn, T. Samad, S. Glavaski, I. Hiskens, and J. Stoustrup, eds.), Berlin: Springer-Verlag, 2017.

[17] A. Dominguez, L. A. Barragan, J. I. Artigas, A. Otin, I. Urriza, and D. Navarro, "Reduced-order models of series resonant inverters in induction heating applications," *IEEE Transactions on Power Electronics*, vol. 32, pp. 2300–2311, March 2017.

[18] N. Femia, G. Spagnuolo, and V. Tucci, "State-space models and order reduction for dc-dc switching converters in discontinuous modes," *IEEE Transactions on Power Electronics*, vol. 10, pp. 640–650, November 1995.

[19] M. Chen and J. Sun, "Reduced-order averaged modeling of active-clamp converters," *IEEE Transactions on Power Electronics*, vol. 21, pp. 487–494, March 2006.

[20] K. Zhang, Z. Shan, and J. Jatskevich, "Large- and small-signal average-value modeling of dual-active-bridge dc-dc converter considering power losses," *IEEE Transactions on Power Electronics*, vol. 32, pp. 1964–1974, March 2017.
[21] G. G. Richards and O. T. Tan, "Decomposed, reduced order model for double-cage induction machines," *IEEE Transactions on Energy Conversion*, vol. EC-1, pp. 87–93, September 1986.
[22] F. D. Rodriguez and O. Wasynczuk, "A refined method of deriving reduced order models of induction machines," *IEEE Transactions on Energy Conversion*, vol. EC-2, pp. 31–37, March 1987.
[23] P. J. Hart, R. H. Lasseter, and T. M. Jahns, "Reduced-order harmonic modeling and analysis of droop-controlled distributed generation networks," in *IEEE 7th International Symposium on Power Electronics for Distributed Generation Systems (PEDG)*, pp. 1–9, June 2016.
[24] P. J. Hart, R. H. Lasseter, and T. M. Jahns, "Enforcing coherency in droop-controlled inverter networks through use of advanced voltage regulation and virtual impedance," in *2017 IEEE Energy Conversion Congress and Exposition (ECCE)*, pp. 3367–3374, October 2017.
[25] C. Li, J. Xu, and C. Zhao, "A coherency-based equivalence method for mmc inverters using virtual synchronous generator control," *IEEE Transactions on Power Delivery*, vol. 31, pp. 1369–1378, June 2016.
[26] V. Purba, S. V. Dhople, S. Jafarpour, F. Bullo, and B. B. Johnson, "Reduced-order structure-preserving model for parallel-connected three-phase grid-tied inverters," in *2017 IEEE 18th Workshop on Control and Modeling for Power Electronics (COMPEL)*, pp. 1–7, July 2017.
[27] V. Purba, S. V. Dhople, S. Jafarpour, F. Bullo, and B. B. Johnson, "Network-cognizant model reduction of grid-tied three-phase inverters," in *2017 55th Annual Allerton Conference on Communication, Control, and Computing (Allerton)*, pp. 157–164, October 2017.
[28] M. Ebrahimi, H. R. Karshenas, and M. Hassanzahraee, "Comparison of orthogonal quantity generation methods used in single-phase grid-connected inverters," in *IECON 2012 - 38th Annual Conference on IEEE Industrial Electronics Society*, pp. 5932–5937, October 2012.
[29] A. Yazdani and R. Iravani, *Voltage-Sourced Converters in Power Systems*. Hoboken, NJ: John Wiley & Sons, Inc., 2010.
[30] M. K. Kazimierczuk and L. A. Starman, "Dynamic performance of pwm dc-dc boost converter with input voltage feedforward control," *IEEE Transactions on Circuits and Systems I: Fundamental Theory and Applications*, vol. 46, pp. 1473–1481, December 1999.

Victor Purba (S'15) received the Bachelor's and M.S. degrees in electrical engineering in 2014 and 2016, respectively, from University of Minnesota, Minneapolis, MN, USA, where he is currently pursuing the Ph.D. degree in electrical engineering. His research interests include modeling, analysis, and control of power systems with the integration of renewable energy sources.

Brian Johnson (S'08, M'13) obtained the M.S. and Ph.D. degrees in Electrical and Computer Engineering from the University of Illinois at Urbana-Champaign, Urbana, in 2010 and 2013, respectively. He is the Washington Research Foundation Innovation Assistant Professor within the Department of Electrical and Computer Engineering at the University of Washington. Prior to joining the University of Washington in 2018, he was an engineer with the National Renewable Energy Laboratory in Golden, CO. He was awarded a National Science Foundation Graduate Research Fellowship in 2010, and currently serves as an Associate Editor for the IEEE Transactions on Energy Conversion. His research interests are in renewable energy systems, power electronics, and control systems.

Miguel Rodriguez (S'06, M'11) was born in Gijon, Spain, in 1982. He received the M.S. and Ph.D. degrees in telecommunication engineering from the University of Oviedo, Oviedo, Spain, in 2006 and 2011, respectively. From 2011 to 2013, he was a Post-Doctoral Research Associate with the Colorado Power Electronics Center, University of Colorado at Boulder, Boulder, CO, USA. In 2013 he joined Advanced Micro Devices, Inc., in Fort Collins, CO, USA, as a member of the Low Power Advanced Development Group. His current research interests include dc/dc conversion and digital control, analysis of power delivery networks, and linear and switched integrated voltage regulators for microprocessors and SoCs.

Saber Jafarpour (M'16) is a Postdoctoral researcher with the Center for Control, Dynamical Systems and Computation at the University of California, Santa Barbara. He received his Ph.D. in 2016 from the Department of Mathematics and Statistics at Queen's University. His research interests focus on network systems and synchronization of coupled oscillators with application to power grids.

Francesco Bullo (S'95, M'99, SM'03, F'10) is a Professor with the Mechanical Engineering Department and the Center for Control, Dynamical Systems and Computation at the University of California, Santa Barbara. He was previously associated with the University of Padova (Laurea degree in Electrical Engineering, 1994), the California Institute of Technology (Ph.D. degree in Control and Dynamical Systems, 1999), and the University of Illinois. His research interests focus on network systems and distributed control with application to robotic coordination, power grids and social networks. He is the coauthor of "Geometric Control of Mechanical Systems" (Springer, 2004) and "Distributed Control of Robotic Networks" (Princeton, 2009); his "Lectures on Network Systems" (CreateSpace, 2018) is available on his website. He is a Fellow of IEEE and IFAC. He has served on the editorial boards of IEEE, SIAM, and ESAIM journals, and serves as 2018 IEEE CSS President.

Sairaj V. Dhople (M'13) received the B.S., M.S., and Ph.D. degrees in electrical engineering from the University of Illinois at Urbana-Champaign, Urbana, IL, USA, in 2007, 2009, and 2012, respectively. He is currently an Associate Professor with the Department of Electrical and Computer Engineering, University of Minnesota, Minneapolis, MN, USA, where he is with the Power and Energy Systems research group. His research interests include modeling, analysis, and control of power electronics and power systems with a focus on renewable integration. Dr. Dhople received the National Science Foundation CAREER Award in 2015. He is an Associate Editor for the IEEE Transactions on Energy Conversion and the IEEE Transactions on Power Systems.